Endothelial CD99 signals through soluble adenylyl cyclase and PKA to regulate leukocyte transendothelial migration

Richard L. Watson,[1] Jochen Buck,[2] Lonny R. Levin,[2] Ryan C. Winger,[1] Jing Wang,[3] Hisashi Arase,[3] and William A. Muller[1]

[1]Department of Pathology, Feinberg School of Medicine, Northwestern University, Chicago, IL 60208
[2]Department of Pharmacology, Weill Medical College of Cornell University, New York, NY 10065
[3]Laboratory of Immunochemistry, WPI Immunology Frontier Research Center and Department of Immunochemistry, Research Institute for Microbial Diseases, Osaka University, Osaka 565-0871, Japan

CD99 is a critical regulator of leukocyte transendothelial migration (TEM). How CD99 signals during this process remains unknown. We show that during TEM, endothelial cell (EC) CD99 activates protein kinase A (PKA) via a signaling complex formed with the lysine-rich juxtamembrane cytoplasmic tail of CD99, the A-kinase anchoring protein ezrin, and soluble adenylyl cyclase (sAC). PKA then stimulates membrane trafficking from the lateral border recycling compartment to sites of TEM, facilitating the passage of leukocytes across the endothelium. Pharmacologic or genetic inhibition of EC sAC or PKA, like CD99 blockade, arrests neutrophils and monocytes partway through EC junctions, in vitro and in vivo, without affecting leukocyte adhesion or the expression of relevant cellular adhesion molecules. This is the first description of the CD99 signaling pathway in TEM as well as the first demonstration of a role for sAC in leukocyte TEM.

CORRESPONDENCE
William A. Muller:
wamuller@northwestern.edu

Abbreviations used: AC, adenylyl cyclase; AKAP, A-kinase anchoring protein; CREB, cAMP response element-binding protein; ddAdo, 2′5′-dideoxyadenosine; DMSO, dimethylsulfoxide; EC, endothelial cell; GαM, goat anti–mouse; HUVEC, human umbilical vein EC; LBRC, lateral border recycling compartment; MHEC, mouse heart EC; PBMC, peripheral blood mononuclear cell; PGE_2, prostaglandin E_2; PKI, protein kinase inhibitor peptide; PMN, polymorphonuclear leukocyte; sAC, soluble AC; sAC_{fl}, full-length sAC; sAC_t, truncated sAC; TEM, transendothelial migration; tmAC, transmembrane AC; TR, targeted recycling.

During inflammation, leukocytes are recruited to sites of tissue damage through a series of adhesive molecular interactions between leukocytes in circulation and the endothelium (Ley et al., 2007; Muller, 2011). Transendothelial migration (TEM), or diapedesis, is the step in which leukocytes traverse the endothelial barrier to gain access to the interstitium. Two membrane proteins critical for this process are platelet/endothelial cell (EC) adhesion molecule-1 (PECAM) and CD99. The role of CD99 in TEM has been established for monocytes, neutrophils, and T cells both in vitro (Schenkel et al., 2002; Lou et al., 2007; Manes and Pober, 2011) and in vivo (Bixel et al., 2004; Dufour et al., 2008; Bixel et al., 2010). However, the mechanism by which EC CD99 regulates TEM is unknown.

PECAM and CD99 are expressed on most hematopoietic cells and are concentrated along endothelial borders (Ley et al., 2007; Muller, 2011). These proteins interact homophilically between leukocytes and ECs to regulate TEM sequentially in vitro, with PECAM acting upstream of CD99 (Schenkel et al., 2002; Lou et al., 2007; Sullivan et al., 2013); inhibiting PECAM arrests leukocytes apically over EC borders, whereas disruption of CD99 arrests leukocytes partially through the junction (Schenkel et al., 2002; Lou et al., 2007). Pools of unligated PECAM, CD99, and other molecules relevant to TEM reside in the lateral border recycling compartment (LBRC), and membrane from this compartment is directed to sites of TEM in a process known as targeted recycling (TR; Mamdouh et al., 2003, 2008). Whereas PECAM–PECAM interaction is known to be critical for TR, and subsequently TEM (Mamdouh et al., 2003), the role of CD99 in the recruitment of the LBRC is unknown.

CD99 is a unique, small (32-kD) glycoprotein that is homologous only to the recently described CD99L2 (32% sequence homology; Suh et al., 2003). The cytoplasmic tail of CD99 is short and is not known to interact with any

J. Wang's present address is Dept. of Physiology and Pharmacology, University of Calgary, Calgary, Alberta T2N 4N1, Canada.

The Rockefeller University Press $30.00
J. Exp. Med. 2015 Vol. 212 No. 7 1021–1041
www.jem.org/cgi/doi/10.1084/jem.20150354

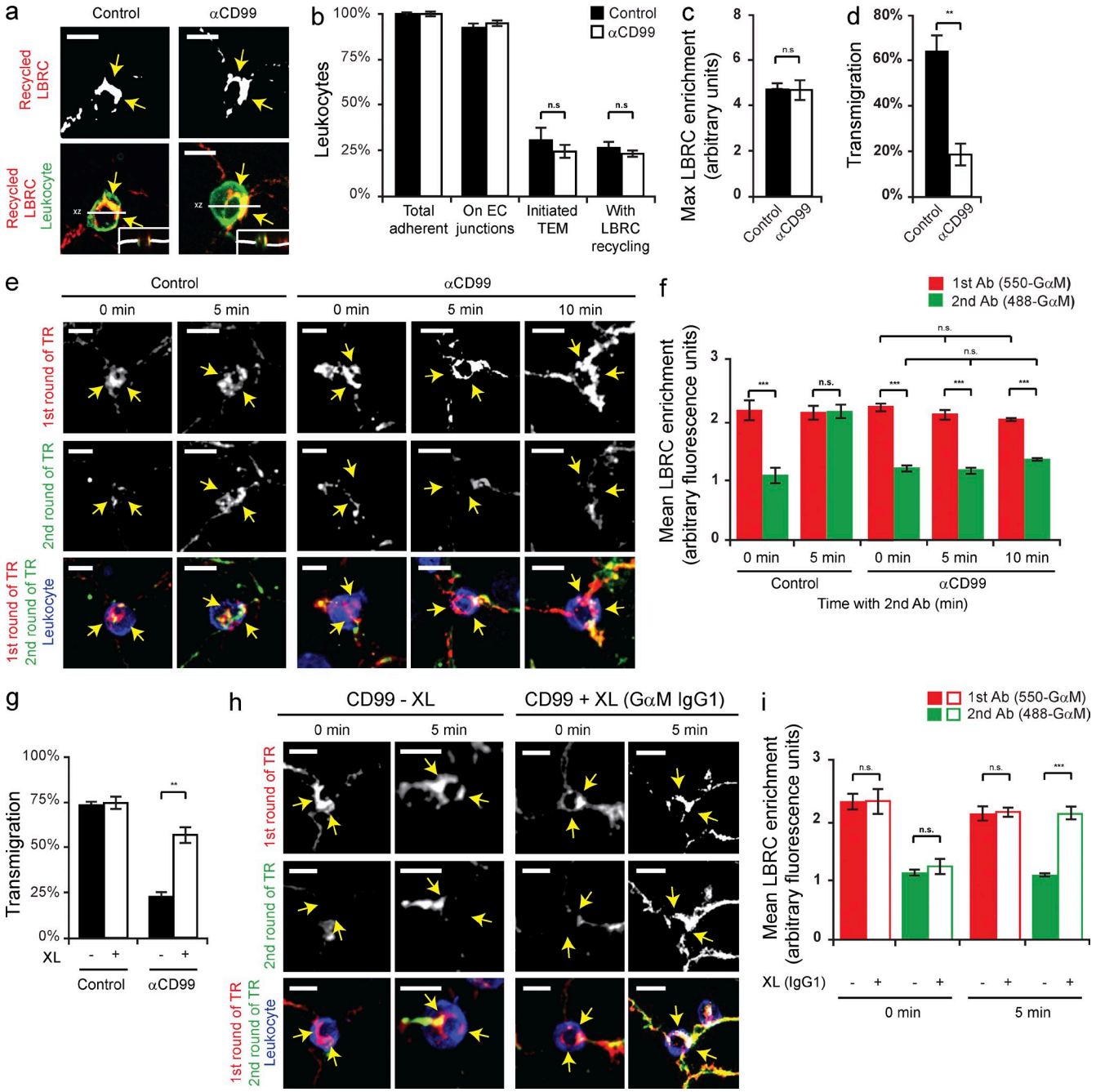

Figure 1. CD99 engagement stimulates a second wave of TR to sites of transmigration. (a) TR assays were performed (see Materials and methods) in presence of either anti-CD99 mAb (IgG_1) or mouse IgG_1 (control). Arrows denote LBRC enrichment. Insets show xz-orthogonal view. (b) Quantification of results. Values represent percent of leukocytes per field of view. (c) LBRC enrichment was quantified as previously described (Mamdouh et al., 2003). In brief, the maximum fluorescence intensity (MFI) around the leukocyte was divided by the MFI of staining along neighboring junctions not in contact with leukocytes. Values greater than one denote enrichment. (d) Quantitative TEM assays were performed in parallel to ensure that anti-CD99 blocked TEM. (e) Two-color TR assays (see Materials and methods) were performed in the continuous presence of anti-CD99 (IgG_1) or mouse IgG_1 (control). DyLight550 GαM IgG_{2a} (550-GαM IgG_{2a}, first antibody) labeled LBRC membrane (labeled with nonblocking mouse anti-PECAM IgG_{2a} antibody, clone P1.1) that trafficked before the CD99-dependent step of TEM. DyLight488 GαM IgG_{2a} (GαM IgG_{2a}, second antibody) labeled LBRC membrane (labeled with P1.1 antibody) delivered after leukocytes have been arrested by anti-CD99. Time denotes minutes incubated with 488-GαM_{2a}. (f) Quantification of LBRC enrichment was performed for both antibodies as a function of time. In brief, the average MFI around the leukocyte was divided by the MFI of neighboring junctional staining for each antibody. (g) TEM assays were performed using HUVECs pretreated with either anti–VE-cadherin (nonblocking, control) or anti-CD99. After 50 min, either GαM (GαM IgG, cross-linking secondary antibody, XL) or goat anti–rabbit (GαRb IgG, control) was added to the cells for 10 min. (h) Two-color TR assays were performed in the presence of anti-CD99 mAb (IgG_1, as described above). Before incubation of samples with

other proteins. Much is known about the signaling mechanisms of other EC adhesion molecules (Muller, 2011), but nothing to date has been published regarding the downstream signaling mechanisms of CD99.

In this study, we found that CD99 and soluble adenylyl cyclase (sAC) interact at endothelial borders with PKA through the A-kinase anchoring protein (AKAP) ezrin. The formation of this signaling complex is dependent on a small lysine-rich region of the CD99 cytoplasmic tail. During TEM, homophilic engagement of endothelial CD99 leads to activation of PKA through sAC, which triggers TR of the LBRC to sites of TEM.

RESULTS

CD99 engagement stimulates a second wave of TR to sites of TEM

Abolishing PECAM function has been previously shown to inhibit the targeted enrichment of LBRC membrane to sites of TEM, thus preventing TEM (Mamdouh et al., 2003). Because CD99 is also a resident molecule of the LBRC and it functions downstream of PECAM during TEM, we hypothesized that CD99 is required for a subsequent step in TR. To test this, we used a specialized technique to monitor LBRC membrane movement during TEM, known as the TR assay (see Materials and methods; Mamdouh et al., 2003; Mamdouh et al., 2008). In brief, this technique utilizes PECAM as a surrogate marker for the LBRC. We used a Fab fragment of a nonfunctional blocking antibody (mouse anti–human PECAM, clone P1.1 (Liao et al., 1995), to prebind PECAM in the LBRC. Any P1.1 Fab on the surface is saturated with unlabeled anti–mouse IgG at 4°C. We are then able to track the movement of the LBRC during TEM using the identical anti–mouse IgG conjugated to a fluorophore. To test our hypothesis, target recycling assays were performed using ECs pretreated with either anti-CD99 mAb or control IgG. Despite blocking transmigration with anti-CD99, a similar percentage of leukocytes were enriched with membrane from the LBRC (Fig. 1, a–d). (Definition of LBRC enrichment is a >1 fold increase in the staining around a leukocyte compared with a neighboring junction not in contact with the leukocyte.) From this, we concluded that CD99 is not required for the initiation of TR of the LBRC. However, this is not surprising given the phenotype of anti-CD99 blockade.

Because blocking CD99 function did not inhibit the initiation of TR, we next sought to test whether the ablation of CD99 function blocks TEM by preventing subsequent recruitment of the LBRC. To test this hypothesis, we used a modified TR assay (see Materials and methods). In brief, we used two different secondary antibodies to monitor the movement of membrane from the LBRC (assessed by PECAM labeled with a nonfunctional blocking mAb): DyLight550-conjugated goat anti–mouse secondary (550-GαM) to label membrane delivered before the CD99-dependent step of TEM, and DyLight488-GαM (488-GαM) to label LBRC membrane delivered after leukocytes have been blocked at the CD99-dependent step of TEM. Using this technique, we found that although leukocytes arrested by anti-CD99 mAb showed enrichment for LBRC membrane delivered before the CD99-dependent step of TEM (as seen by enrichment of the 550-GαM antibody), blocking CD99 function prevented further delivery of the LBRC to sites of EC–leukocyte contact (as seen by absence of enrichment with the 488-GαM antibody; Fig. 1, e and f). As a control, ECs pretreated with IgG control demonstrated LBRC enrichment with both antibodies. Therefore, we conclude that CD99 is required for additional membrane recruitment from the LBRC, and that blocking CD99 function prevented subsequent influx of the LBRC to sites of TEM where leukocytes were arrested.

Anti-CD99 mAb inhibits TEM by disrupting the engagement of leukocyte CD99 with endothelial CD99, thus preventing the multivalent clustering of CD99 on each cell type and the subsequent activation of downstream effector molecules. In EC, anti-CD99 prevents recruitment of the LBRC, thus blocking TEM. We postulated that artificially clustering endothelial CD99 could bypass the antibody blockade by providing the necessary signal to restore TR and TEM. To test this hypothesis, we first blocked TEM by pretreating the EC with anti-CD99 (IgG_1 mAb) and then adding GαM IgG_1 (cross-linking IgG) or goat anti–rabbit IgG (control IgG). Addition of the cross-linking IgG specifically restored TR and TEM, despite the presence of continued anti-CD99 blockade (Fig. 1, g–i). Thus, clustering of endothelial CD99 is sufficient to initiate a signal to recruit the LBRC.

CD99 engagement activates PKA

The cytoplasmic tail of CD99 is bereft of traditional signaling domains. To find potential signaling pathways responsible for restoring TR, we investigated whether compounds known to stimulate EC membrane movement, such as histamine (Feng et al., 1996), were sufficient to induce TR and rescue TEM in the presence of anti-CD99. We performed TEM assays in which HUVECs were blocked with anti-PECAM or anti-CD99 and then briefly treated with histamine. Histamine selectively overcame the CD99 blockade and significantly restored TEM (Fig. 2 a). Because histamine acts on three receptors in EC (H3-receptor is predominately neuronal), we used pharmacologic antagonists of each receptor to show that blocking the EC H2-receptor (H2-R) specifically prevented the ability of histamine to overcome the CD99 blockade (Fig. 2 b). The H2-R agonist dimaprit reproduced the

488-GαM IgG_{2a} at 37°C, cells were treated with either GαM IgG_1 (CD99-specific cross-linking antibody) or GαRb IgG for 0 or 5 min. (i) Degree of LBRC enrichment was quantified. Bars, 10 µm. Images are representative of three (a and h) or four (e) independent experiments. Data represent the mean value of three (b–d, f, and i) or four (g) independent experiments. Error bars denote SEM. **, $P < 0.01$; ***, $P < 0.001$; Student's *t* test).

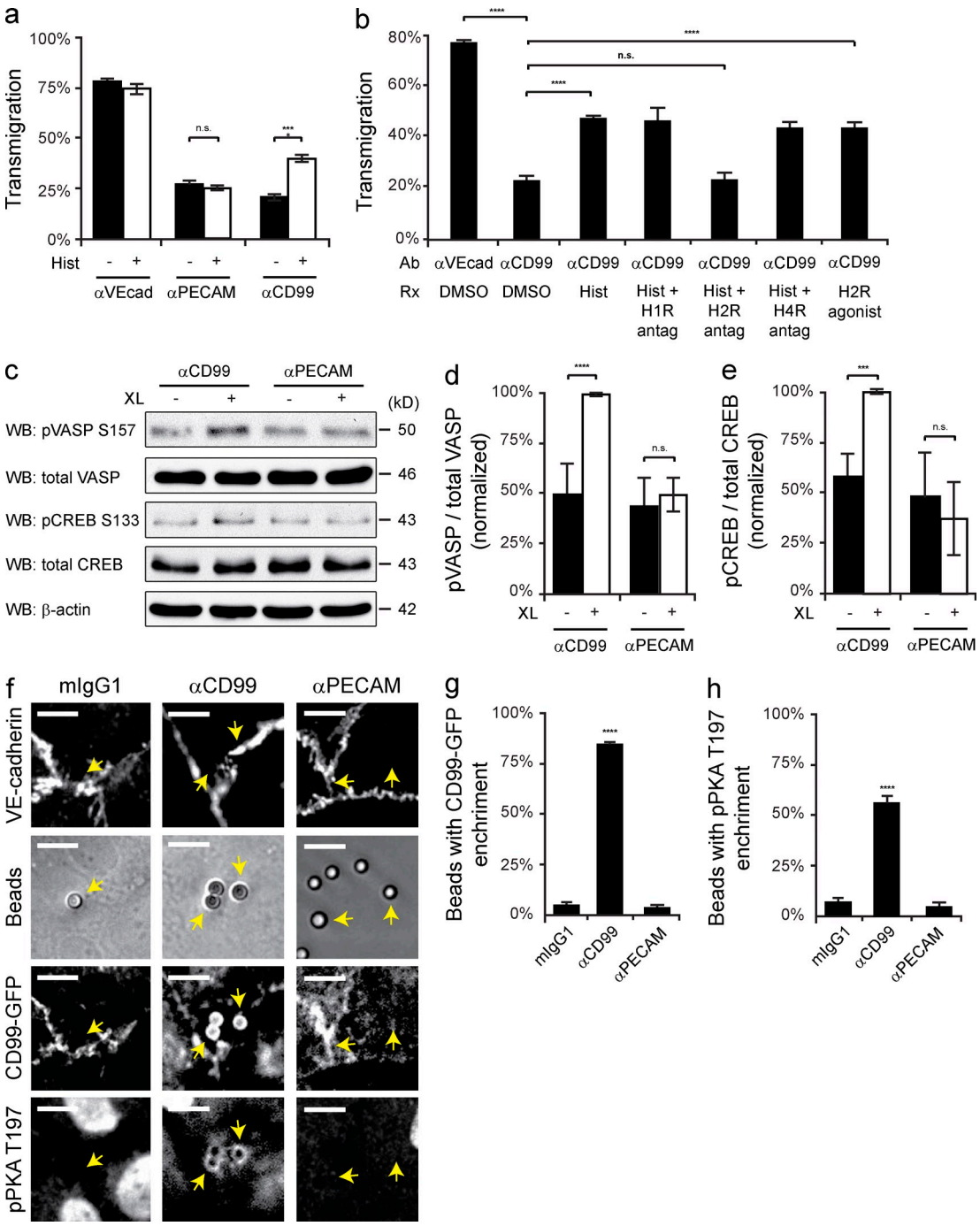

Figure 2. Engagement of EC CD99 activates PKA. (a) Quantitative TEM assays were performed using HUVECs pretreated with nonblocking anti–VE-cadherin, anti-PECAM, or anti-CD99 mAb. After 50 min, histamine (10 µM) was added to samples for 10 min at 37°C. (b) TEM assays were performed using HUVECs pretreated with either anti–VE-cadherin (nonblocking control) or anti-CD99 mAb. Additionally, HUVECs were pretreated with diphenhydramine (H1-R antagonist, 10 µM), ranitidine (H2-R antagonist, 10 µM), or JNJ-10191584 (H4-R antagonist, 10 µM) or DMSO (carrier). After 50 min, histamine (10 µM) or dimaprit (H2-R agonist, 10 µM) was added to samples for 10 min. (c) Immunoblot analysis of phospho-VASP S157 and phospho-CREB S133 activity after anti-CD99 or anti-PECAM mAb (control) cross-linking (XL) in resting HUVECs. (d and e) Quantification of results in c, pVASP and pCREB signals were normalized to total VASP and total CREB, respectively. Values were then normalized to CD99 XL. (f) Antibody-coated polystyrene bead recruitment of CD99 and activation of phospho-PKA. Beads precoupled with $mIgG_1$, anti-CD99 mAb, or anti-PECAM mAb were added to HUVEC monolayers expressing hCD99-GFP. Monolayers were subsequently stained with anti–VE-cadherin and anti-pPKA T197 PKA antibodies. Arrows indicate beads bound to HUVECs. (g and h) Quantification of data; percent of beads in the field of view with either hCD99-GFP or pPKA T197 enrichment. Bars, 10 µm. Images are representative of three (f) or four (c) independent experiments. Numerical values are the mean of three (a, b, e, g, and h) or four (d) independent experiments. Error bars represent SD (d and e) or SEM (a, b, g, and h; ***, $P < 0.001$; ****, $P < 0.0001$; Student's *t* test [a, b, d, and e] and ANOVA [g and h]).

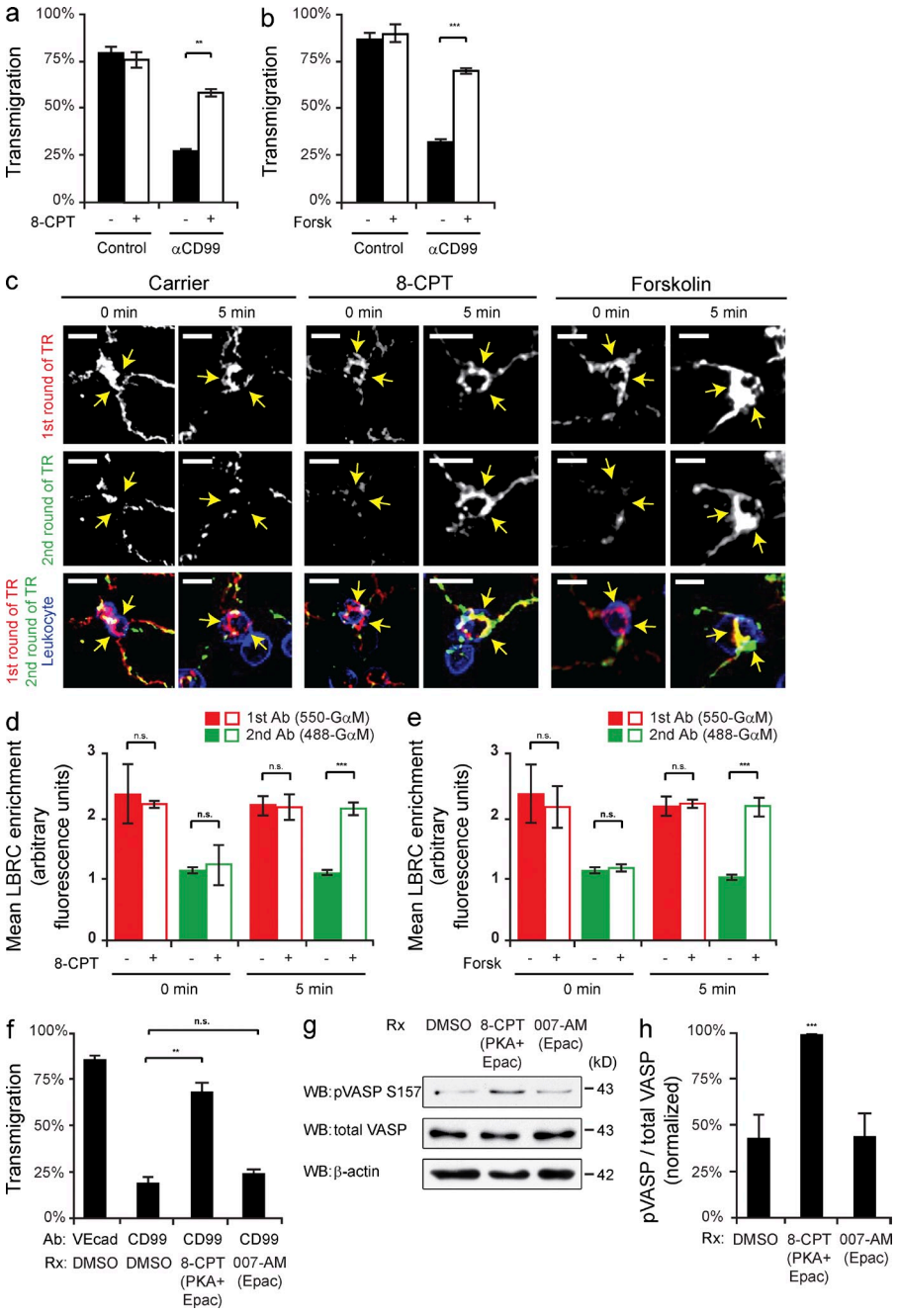

Figure 3. Raising intracellular cAMP reverses anti-CD99 blockade of transmigration and restores TR of the LBRC. (a and b) Quantitative TEM assays were performed using HUVECs pretreated with anti–VE-cadherin (control) or anti-CD99 mAb (IgG_1). After 50 min, 8-CPT (30 µM), Forskolin (30 µM), or DMSO (control) was added to the cells for 10 min. (c) Two-color TR assays were performed (as previously described). In brief, before warming monolayers to 37°C, 488-GαM IgG_{2a} and 8-CPT, Forskolin, or DMSO were added. Cells were then incubated at 37°C for either 0 or 5 min and subsequently washed, fixed, and stained. Arrows denote LBRC enrichment around anti-CD99–arrested monocytes. (d and e) LBRC enrichment was quantified for both 550- or 488-GαM antibodies. (f) Quantitative TEM assays were performed using HUVECs pretreated with either anti–VE-cadherin (control) or anti-CD99 mAb. PBMCs were then added and allowed to transmigrate at 37°C for 50 min. 10 min before fixation, either 8-CPT (general cAMP analogue) or 007-AM (selective-Epac activator) was added to cells. (g) HUVECs were treated in parallel with either 8-CPT or 007-AM for 10 min and then lysed. Immunoblot analysis of pVASP-S157 normalized to total VASP was used to assess PKA activity induced by the drugs. (h) Quantification of results above. Bars, 10 µm. Images are representative of two (c) or three (g) independent experiments. Numerical values are the average of two (d and e) or three (a, b, f, and h) independent experiments. Error bars represent SD (h) or SEM (a, b, and d–f; **, $P < 0.01$; ***, $P < 0.001$; Student's *t* test [a, b, and d–f] and ANOVA [h]).

effect of histamine by overcoming anti-CD99 treatment. We conclude that the ability of histamine to override the anti-CD99 blockade of TEM was a result of the activation of a common downstream signaling pathway shared by H2-R and CD99.

H2-R activation induces cAMP production and subsequent PKA activation (Forte and Zhu, 2010). We tested whether CD99 engagement could reproduce this effect. HUVECs were cross-linked with anti-CD99 or anti-PECAM mAb, using two known PKA substrates, phospho-VASP Ser157 (Butt et al., 1994; Howe et al., 2005) and phospho-cAMP response element-binding protein (CREB) Ser133 (Gonzalez and Montminy, 1989), to assess PKA activity. Immunoblot analysis revealed that cross-linking CD99 selectively activated PKA (Fig. 2, c–e).

To gain further understanding of how CD99 clustering activates PKA, we used antibody-coated beads in conjunction with immunofluorescence (IF) staining to spatially assess PKA activity. Phosphorylation of Thr197 of the PKA-Cα subunit is required for PKA activity (Cauthron et al., 1998). Although constitutively phosphorylated in mammalian cells, phospho-PKA Thr197 can be used as a marker for locally activated PKA in intact cells. Upon activation of PKA by cAMP, the tetrameric holoenzyme dissociates, permitting access of the antibody to this residue once hidden by the regulatory

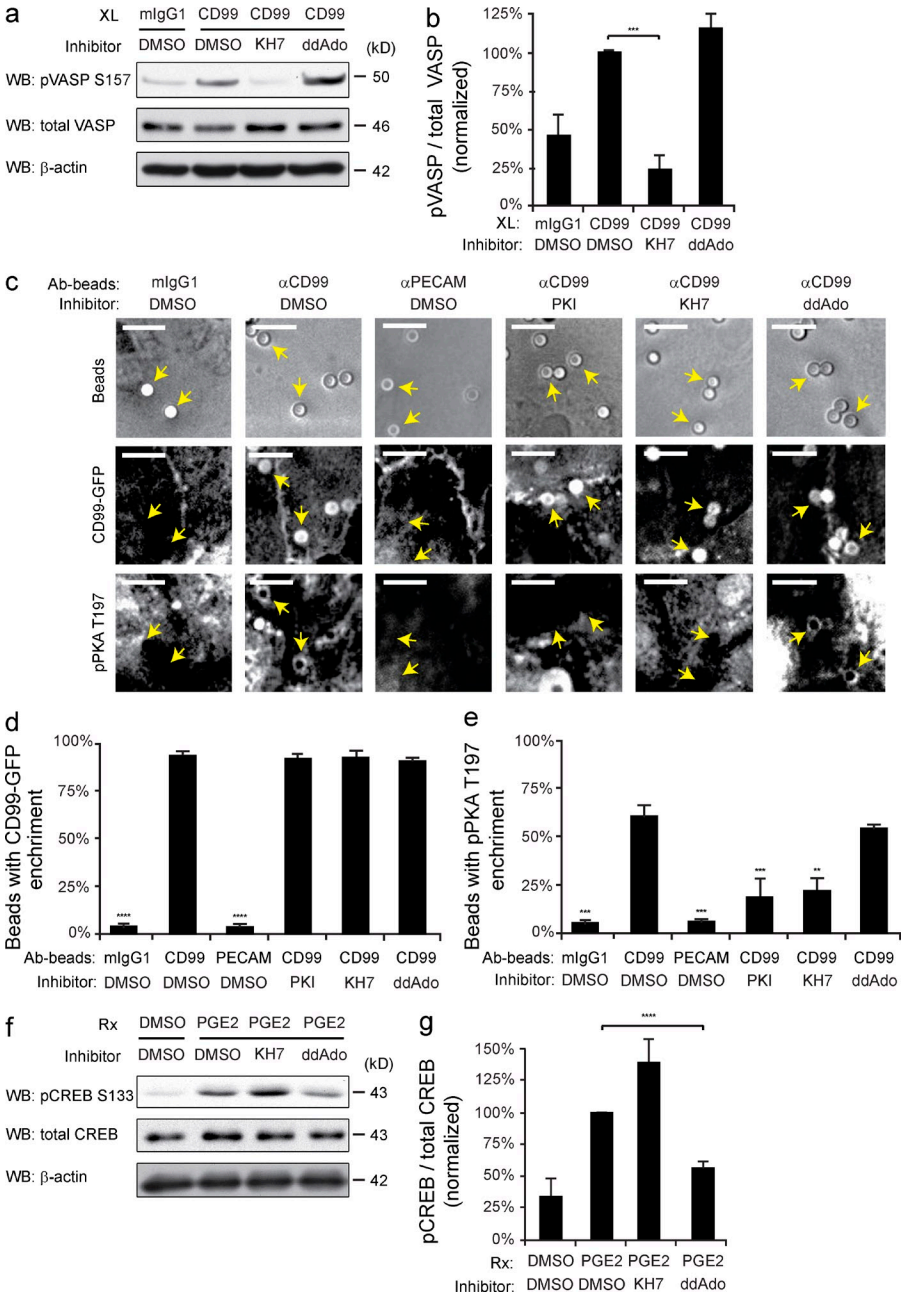

Figure 4. Inhibition of sAC prevents CD99 activation of PKA. (a) HUVECs were pretreated with 50 µM KH7 (sAC inhibitor), 25 µM ddAdo (tmAC inhibitor), or DMSO (control). HUVECs were then cross-linked with $mIgG_1$ control or anti-CD99 and lysed. Immunoblot analysis was performed for pVASP-S157 and total VASP. (b) Quantification of immunoblots. Values denote pVASP-S157 signal normalized to total VASP signal. Values were then normalized to the CD99/DMSO condition. (c) Amine-modified polystyrene latex beads were precoupled with $mIgG_1$, anti-CD99, or anti-PECAM. HUVECs expressing hCD99-GFP were pretreated with DMSO, PKI, KH7, or ddAdo. Beads were added to HUVECs for 20 min at 37°C. Samples were then fixed and stained for VE-cadherin (not depicted) and pPKA-T197. Arrows indicate where polystyrene beads bound to HUVECs. (d and e) Data were quantified for percent of beads in the field of view with either hCD99-GFP or pPKA-T197 enrichment. (f) HUVECs were pretreated with DMSO, KH7, or ddAdo. PGE_2 (100 ng/ml) was added to HUVECs for 10 min. Cells were then lysed and immunoblot analysis was performed for pCREB-S133 and total CREB. (g) Quantification of immunoblots. Values denote pCREB-S133 signal normalized to total CREB signal. Values for all conditions were then normalized to DMSO/PGE_2 condition. Bars, 10 µm. Images are representative of two (c), three (f), or four (a) independent experiments. Numerical values are the average of two (d and e), three (g) four (b) independent experiments. Error bars represent SD (b) or SEM (d, e, and g; **, $P < 0.01$; ***, $P < 0.001$; ****, $P < 0.0001$; Student's *t* test [b] and ANOVA [d, e, and g]).

subunit (Kim et al., 2005a; Taylor et al., 2013). To confirm that the anti-CD99–coated beads were recruiting EC CD99, HUVECs were infected with adenovirus encoding CD99-GFP. In accordance with our immunoblot analysis, beads coated with anti-CD99 specifically recruited endothelial CD99-GFP and activated PKA, whereas beads bearing anti-PECAM or $mIgG_1$ did neither (Fig. 2, f–h). To ensure the positive phospho-PKA signal was not caused by autofluorescence of the beads, HUVECs were also stained with VE-cadherin, which showed no enrichment. Together, these data demonstrate that the polyvalent engagement of endothelial CD99 activates PKA.

Raising intracellular cAMP reverses anti-CD99 blockade of transmigration

Because there are cAMP-independent ways to activate PKA (Niu et al., 2001; Ferraris et al., 2002), we determined if elevating cAMP could restore transmigration in EC blocked with anti-CD99. We performed TEM assays in which HUVECs were pretreated with either nonblocking anti–VE-cadherin (control) or anti-CD99 mAb. Brief treatment with either 8-CPT (a cAMP analogue) or Forskolin (an activator of ACs) restored TEM in anti-CD99 blocked cells to control levels (Fig. 3, a and b). Next, we examined if 8-CPT and Forskolin could also rescued membrane trafficking from the LBRC.

We found that within 5 min either 8-CPT or Forskolin restored TR to sites of TEM where leukocytes were arrested by anti-CD99 (Fig. 3, c–e). From these data, we inferred that the ability of 8-CPT and Forskolin to overcome anti-CD99 blockade of TEM was due to their ability to activate PKA to induce LBRC membrane trafficking to sites of leukocyte contact.

In addition to the classic PKA pathway, the downstream effects of cAMP can also be mediated by Epac (exchange protein activated by cAMP). This cAMP-regulated guanine exchange factor activates the small GTPase Rap1, which in turn stabilizes VE-cadherin at cell–cell junctions (Fukuhra et al., 2006; Noda et al., 2010). Rapid remodeling of adherens junctions is a critical step for effective transmigration (Muller, 2011), so we investigated whether there was a role for Epac downstream of CD99 signaling. We took advantage of a modified cAMP analogue that selectively activates Epac, 8-CPT-2Me (007-AM;Vliem et al., 2008). HUVECs pretreated with either anti-CD99 or control antibody were briefly treated with either 8-CPT (which can activate both PKA and Epac) or 007-AM (Epac selective cAMP analogue). As observed before, 8-CPT restored TEM in anti-CD99 blocked cells to control levels; however, the Epac-selective cAMP analogue had no effect (Fig. 3 f). Monolayers treated in parallel with the cAMP analogues were used for immunoblot analysis of phospho-VASP. As expected, 8-CPT induced activation of PKA, whereas 007-AM did not (Fig. 3, g and h). These data show that the ability of cAMP to overcome anti-CD99 blockade of TEM is due specifically to the activation of PKA and not Epac.

Inhibition of sAC prevents CD99 activation of PKA

We next investigated how CD99 engagement led to increased cAMP and activated PKA. In mammalian cells, two classes of AC catalyze the formation of cAMP: G protein–regulated transmembrane ACs (tmACs) and sACs (sACs). KH7 is an sAC-specific inhibitor, whereas 2′5′-didexoyadenosine (ddAdo), when used at or below 50 μM, is a tmAC-selective inhibitor (Bitterman et al., 2013). HUVECs were pretreated with KH7, ddAdo, or dimethylsulfoxide (DMSO; control) and cross-linked with anti-CD99 or $mIgG_1$ control. Immunoblot analysis for phospho-VASP was performed to assess PKA activity. The activation of PKA by cross-linking CD99 was significantly attenuated in EC treated with KH7, whereas inhibition of tmACs with ddAdo had no effect (Fig. 4, a and b). To confirm this observation, we used antibody-coated beads and IF staining to spatially assess PKA activity. As seen previously, anti-CD99–coated beads were locally enriched with phospho-PKA staining. Furthermore, activation of PKA was significantly blocked in HUVECs pretreated with KH7 but not with ddAdo. As an additional control, we demonstrated that CD99-coated bead activation of PKA was blocked by the PKA inhibitor myristolyated protein kinase inhibitor peptide (PKI; Fig. 4, c–e). From these data, we conclude that CD99 cross-linking activated PKA via stimulation of sAC.

To ensure that tmACs were being properly inhibited at the concentration of ddAdo used, HUVECs were pretreated as previously described. Cells were then activated with prostaglandin E_2 (PGE_2), a known GPCR ligand that stimulates tmAC production of cAMP. PKA activation was assessed by immunoblot analysis of phospho-CREB. In contrast to CD99 cross-linking, PGE_2-induced activation of PKA was not affected by KH7 but was significantly inhibited by ddAdo treatment (Fig. 4, f and g). These data support the finding that endothelial CD99 activation of PKA is due specifically to signaling through sAC.

Inhibiting sAC blocks leukocyte TEM

Having demonstrated that CD99 associates with and signals through sAC to activate PKA, we examined if sAC is required for transmigration. We performed TEM assays in HUVECs pretreated with either anti-CD99 (mouse IgG_1 mAb) or anti–VE-cadherin (mouse IgG_{2a} mAb), as well as PKI, KH7, ddAdo, or DMSO. As seen above, inhibiting endothelial CD99 with function-blocking mAb substantially ablated TEM (Fig. 5 a). As expected (Fig. 1), this blockade could be overcome if GαM cross-linking antibody was briefly (10 min) added to polyvalently cluster the function-blocking CD99 antibody, thus providing the necessary activation to propagate EC CD99 signaling cascade. As a control, adding goat anti–rabbit antibody had no effect on anti-CD99 blockade of TEM. Inhibiting sAC or PKA not only prevented CD99 cross-linking-mediated restoration of TEM, but also blocked TEM in HUVECs treated with control antibody (Fig. 5 a); this is expected if sAC and PKA function sequentially downstream of CD99. Conversely, blocking tmACs did not have any effect on leukocyte TEM.

To further test if sAC and PKA are involved in CD99 signaling in TEM, we examined whether inhibiting sAC arrests leukocytes at a similar step, phenotypically, as anti-CD99. TEM assays were performed in the presence of anti-CD99, PKI, KH7, ddAdo, or DMSO. IF staining was performed on fixed samples. Using 3-D confocal microscopy, we were able to assess where leukocytes were arrested in relation to the endothelial monolayers. As seen from xz-orthogonal views (Fig. 5, b and c), blocking PKA or sAC reproduced the phenotype of the anti-CD99 blockade, in which leukocytes are arrested partway through endothelial junctions. To ensure that this assay properly discerned leukocytes stuck partway through the junctions from those arrested on the apical surface, TEM assays were performed in HUVECs pretreated with either anti-PECAM or anti-CD99. In accordance with previous studies (Schenkel et al., 2002; Lou et al., 2007), anti-PECAM blockade arrested leukocytes on the apical surface of EC, whereas anti-CD99 arrested cells partway through junctions (Fig. 5, d and e). These results were reproduced using TNF-activated HUVEC monolayers, which showed an equal level of blockade for anti-CD99 and KH7-treated conditions, with the majority of leukocyte arrested partway through the endothelial junctions (unpublished data). Eluate controls (Mamdouh et al., 2009) confirmed that

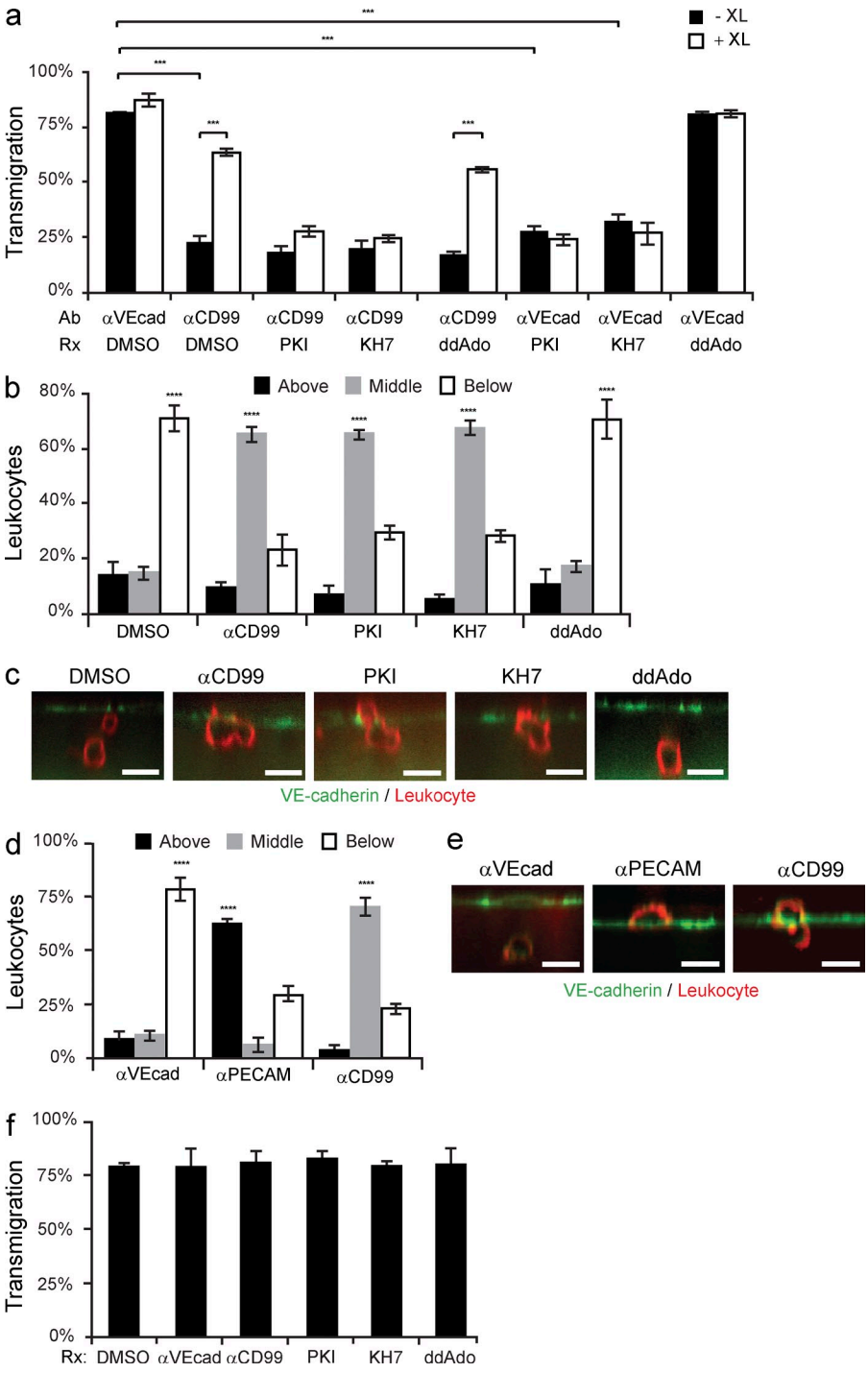

Figure 5. Inhibiting sAC or PKA blocks leukocyte transmigration. (a) TEM assays were performed using HUVECs pretreated with either anti–VE-cadherin or anti-CD99, as well as DMSO, PKI, KH7, or ddAdo. Before fixation, either GαM IgG (cross-linking antibody, XL) or GαRb IgG (control) was added to samples for 10 min (b and c) PBMCs were added to HUVECs pretreated with DMSO, anti-CD99, PKI, KH7, or ddAdo. Samples were stained with anti–VE-cadherin (EC) and anti-CD18 (leukocyte). Confocal images were taken to assess the site of blockade. Leukocytes were scored as being above the endothelium, blocked partway through, or migrated below HUVEC monolayers. (d and e) HUVECs were pretreated with anti–VE-cadherin, anti-PECAM, or anti-CD99. PBMCs were allowed to transmigrate for 1 h. Cells were then fixed, stained, imaged, and analyzed (as described above). (f) Eluate control TEM assays were performed as previously described (Mamdouh et al., 2009). In brief, HUVECs were pretreated with anti–VE-cadherin, anti-CD99, PKI, KH7, ddAdo, or DMSO for the duration of the incubation in blocking experiments. Cells were then washed and fresh media was added to samples. HUVECs were incubated at 37°C for 1 h (the duration of the normal blocking experiments). The media was collected from each well. The eluate media contains all of the inhibitor that would have eluted out of the cultures over the duration of the blocking experiment. PBMCs were resuspended in the eluate media, added to untreated HUVECs, and incubated at 37°C for 1 h. Cells were subsequently fixed and analyzed. Bars, 10 µm. Images are representative of two (e) or three (c) independent experiments. Numerical values are the average of two (d and f) or three (a and b) independent experiments. Error bars represent SEM (***, $P < 0.001$; ****, $P < 0.0001$; Student's *t* test [a] and ANOVA [b, d, and f]).

the drugs were only blocking the EC with no secondary effect on the leukocytes (Fig. 5 f).

To confirm that EC sAC is critical for TEM, we used shRNA to knockdown sAC expression in HUVECs and tested for defects in TEM. Compared with scrambled shRNA (control), sAC shRNA resulted in significantly decreased transmigration (Fig. 6 a). Furthermore, this defect in TEM was rescued by the reexpression of a truncated isoform of sAC (sAC_t; Buck et al., 1999). Important to note, sAC_t was rendered resistant to shRNA-mediated knockdown by introducing multiple silent mutations in the target sequence of sAC_t. Samples for immunoblot analysis were collected in parallel to confirm knockdown and rescue of sAC (Fig. 5, b and c). These data demonstrate that genetic ablation of sAC in EC inhibits leukocyte transmigration.

To assess where sAC shRNA arrested leukocytes, IF staining was performed on fixed TEM samples. Knockdown of sAC arrested the majority of the leukocytes partway through

the junctions, at comparable levels to CD99 shRNA (Fig. 6, d and e). Immunoblot analysis was performed on HUVECs treated in parallel to quantify the knockdown efficiency (Fig. 6, f and g). These experiments were replicated using TNF-activated HUVEC monolayers for both monocytes (peripheral blood mononuclear cells [PBMCs]) and neutrophils (polymorphonuclear leukocytes [PMNs]). Similar to the aforementioned results, genetic knockdown of endothelial sAC blocked both monocyte (Fig. 6 h) and neutrophil transmigration (Fig. 6 i) across cytokine-activated endothelial monolayers. Additionally, immunoblot analysis was performed on samples treated in parallel to ensure that genetic ablation of sAC did not affect ICAM-1 up-regulation and the expression of other cellular adhesion molecules (Fig. 6 j) or the distribution of these molecules (not depicted). From these studies, we confirmed that sAC functions at the same step as CD99 in TEM of monocytes across resting and activated EC, as well as of PMNs across activated endothelium.

CD99, sAC, PKA, and ezrin form a signaling complex to regulate TEM

As CD99 is concentrated at endothelial borders (Schenkel et al., 2002) and signals through sAC to regulate TEM, we examined the subcellular distribution of sAC in EC. HUVECs were infected with adenovirus encoding sAC_t-GFP, fixed, and stained for CD99. sAC_t-GFP was expressed not only throughout the cytoplasm, as previously reported (Zippin et al., 2003), but also partially localized to endothelial junctions (Fig. 7 a).

Given that sAC and CD99 colocalize at EC junctions, we sought to determine if these proteins were interacting. We immunoprecipitated endogenous CD99 or sAC from primary ECs and immunoblotted for each respective protein. Under both conditions, CD99 and sAC co-immunoprecipitated in EC (Fig. 7, b and c).

Because CD99 functions via PKA, we tested if PKA interacted with CD99 and sAC. Immunoblot analysis of immunoprecipitations revealed that the regulatory subunit type IIα (RIIα) of PKA specifically interacted with CD99 and sAC (Fig. 7, b and c). Scaffolding proteins known as AKAPs (Wong and Scott, 2004; Carnegie et al., 2009) bind the regulatory subunits of PKA and compartmentalize it to discrete areas of the cell, along with various effector molecules. One such AKAP that functions at the plasma membrane is ezrin. Immunoblot analysis of CD99 and sAC immunoprecipitations revealed that ezrin specifically interacts with CD99, sAC, and PKA-RIIα (Fig. 7, b and c). As a control for specificity, we checked whether CD99 interacts with other AKAPs known to associate with the plasma membrane, such as AKAP-13 (AKAP-Lbc; Wong and Scott, 2004). Although AKAP-13 is expressed in HUVECs, it does not associate with CD99 (Fig. 7 b).

To determine the relationship in which CD99, sAC, and ezrin interact in ECs, we performed coimmunoprecitation analysis on ECs pretreated with either scrambled or sAC shRNA. In sAC shRNA-treated lysates, sAC expression (~50-kD isoform) was significantly decreased compared with SCR controls (Fig. 7, d and e). An equal decrease was appreciated in the amount of sAC that coimmunoprecipitated with CD99 (Fig. 7, d and f). However, knocking down sAC expression did not affect the amount of ezrin that coimmunoprecipitated with CD99 (Fig. 7, d and g).

We next performed coimmunoprecipitation analysis on cells in which ezrin expression was ablated using shRNA. Knocking down ezrin not only decreased the amount of ezrin coimmunoprecipitating with CD99, but it also resulted in less sAC interacting with CD99 (Fig. 7, h–k). These data demonstrate that CD99 associates with sAC through its interaction with ezrin.

To verify that EC ezrin is critical for leukocyte TEM, we performed transmigration assays using HUVECs pretreated with ezrin shRNA. Ezrin shRNA significantly blocked transmigration to similar levels as CD99 shRNA (Fig. 7 l). Immunoblot analysis was performed on cells treated in parallel to quantify the knockdown efficiency (Fig. 7, m and n). These results were reproduced using TNF-activated HUVEC monolayers, which showed an equal level of blockade for CD99 and ezrin shRNA-treated conditions (unpublished data). From this, we concluded that EC CD99 interacts with sAC and PKA-RIIα through ezrin to regulate leukocyte diapedesis.

CD99 cytoplasmic tail mediates TEM through a positively charged juxtamembrane region

The cytoplasmic tail of CD99 is composed of 39 aa, contains no known signaling motifs, and has no known binding partners. However, within the juxtamembrane cytoplasmic tail there lies a short lysine-rich region that is highly conserved across species (Banting et al., 1989; Ellis et al., 1994; Park et al., 2005). To test the importance of this region for CD99 function, we generated a series of CD99-GFP mutants (Fig. 8 a). Endogenous CD99 was knocked down in HUVECs using shRNA, which decreased TEM significantly. Exogenous CD99-GFP was then reexpressed in these cells. Immunoblot analysis demonstrated sufficient knockdown of endogenous CD99 and comparable levels of reexpression of the rescue constructs (Fig. 8 b). Whereas wild-type CD99-GFP was able to rescue TEM, CD99 lacking the majority of its cytoplasmic tail was unable to do so (Fig. 8 c). Furthermore, mutation of the four juxtamembrane lysine residues (KKKLCFK) to negatively charged glutamic acids (EEELCFE) failed to restore TEM. However, conserving the positive charge of this region by mutating the lysine's residues to arginines (RRRLCFR) brought TEM to wild-type levels. Two point mutations were also tested: a putative PKC site (SHR) and a casein kinase II phosphorylation site (TLLE). CD99 bearing either of these two mutations fully rescued TEM, demonstrating that these residues were not important for CD99 function in TEM. These data prove that the positive charge of the juxtamembrane lysines in the cytoplasmic tail of CD99 are required for its function during TEM.

To test whether the ability of the CD99 cytoplasmic tail to support TEM was a result of its ability to interact with sAC and ezrin, we expressed our GFP constructs in EC and immunoprecipitated CD99. We pulled down only CD99 from the

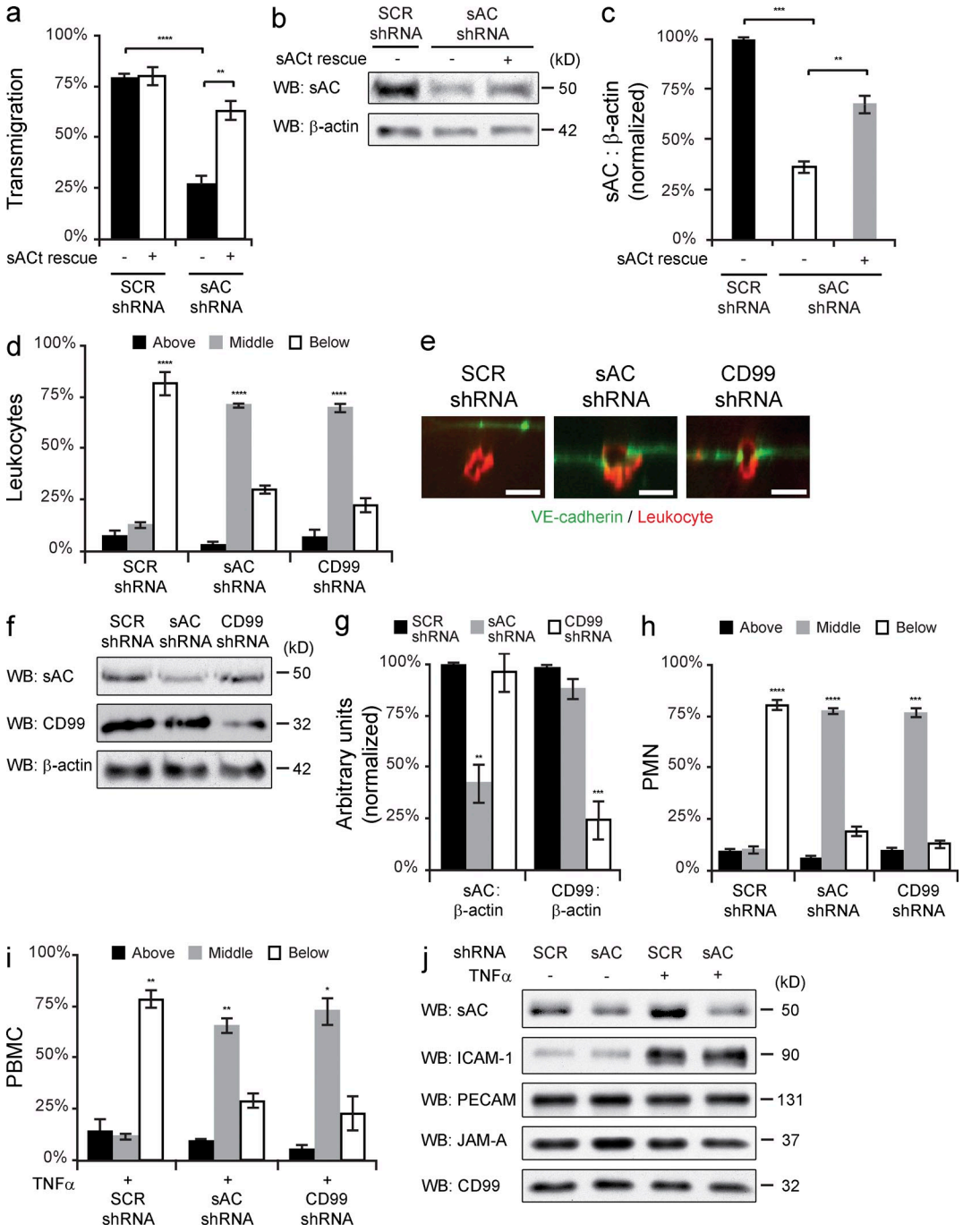

Figure 6. Genetic ablation of endothelial sAC inhibits leukocyte transmigration. (a) Quantitative PBMC TEM assays were performed on HUVECs expressing either scrambled (SCR) or sAC shRNA. Where indicated, the rescue construct (sAC_t) was also expressed. (b) Immunoblot analysis for sAC and β-actin was performed on samples treated in parallel. (c) Quantification of immunoblots. Total sAC expression was normalized to β-actin for each sample and then normalized to SCR control. (d and e) TEM-IF assays were performed on HUVECs expressing SCR, sAC, or CD99 shRNA. (f) Immunoblot analysis for CD99, sAC, and β-actin was performed on samples treated in parallel. (g) Quantification of immunoblots. Total sAC or CD99 expression was normalized to β-actin for each sample and then normalized to SCR control. (h) Quantitative PMN TEM-IF assays were performed on TNF-activated (4 h) HUVECs expressing SCR, sAC, or CD99 shRNA. (i) Quantitative PMBC TEM-IF assays were performed on TNF-activated (4 h) HUVECs expressing SCR, sAC, or CD99 shRNA. (j) Immunoblot analysis of samples treated in parallel were performed for sAC, ICAM-1, PECAM, JAM-A, and CD99 expression. Bars, 10 µm. Images are representative of three (b, e, and j) independent experiments. Numerical values are the mean of two (h and i) or three (a, c, d, and g) independent experiments. Error bars represent SD (c and g) or SEM (a, d, h, and i; *, $P < 0.05$; **, $P < 0.01$; ***, $P < 0.001$; ****, $P < 0.0001$; Student's *t* test [a and c] and ANOVA [d, g, h, and i]).

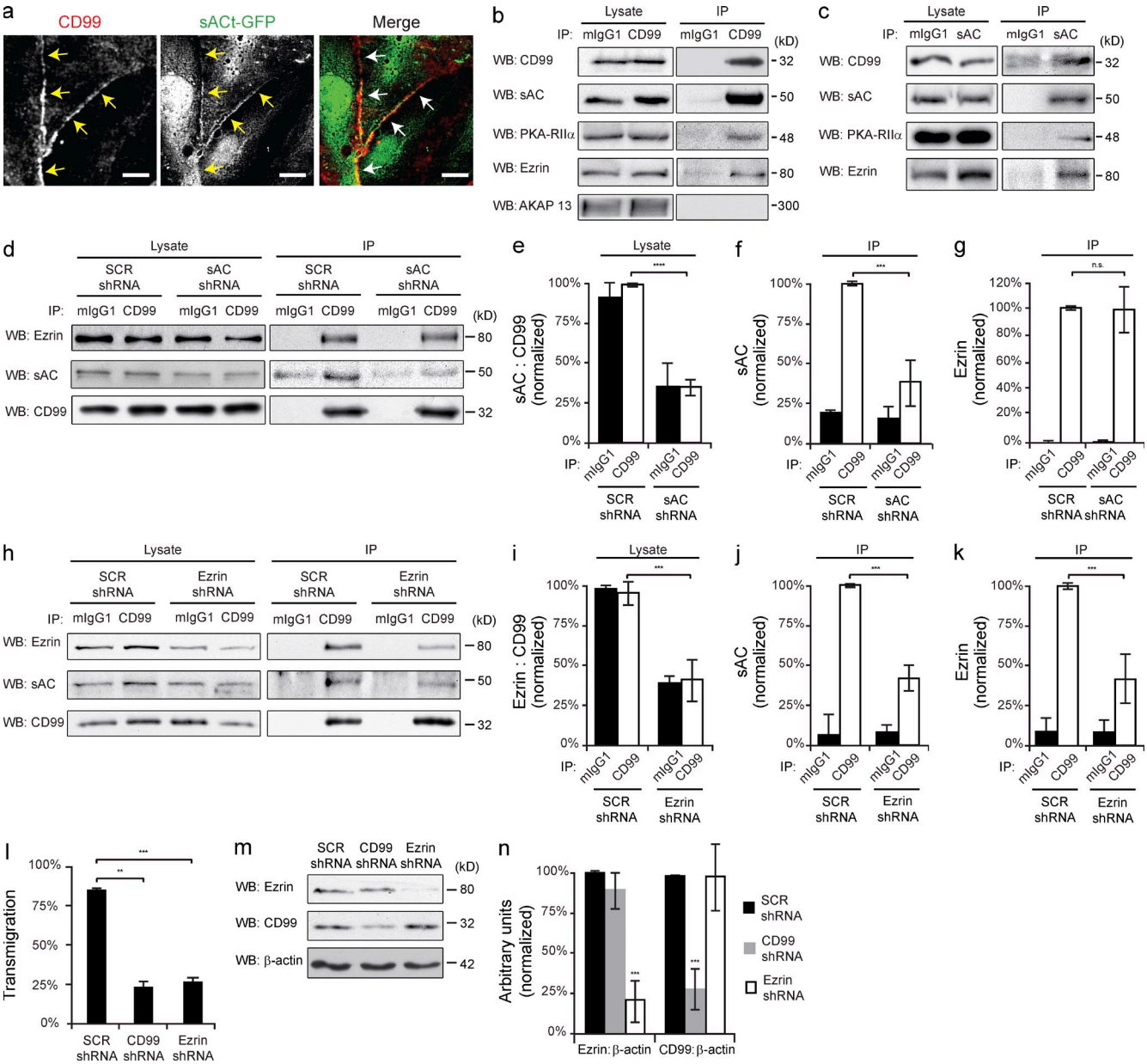

Figure 7. CD99, sAC, PKA, and ezrin form a signaling complex to regulate transmigration. (a) HUVECs were infected with sAC_t-GFP encoding adenovirus. Cells were then fixed and stained for CD99. Arrows denote junctional localization. (b and c) CD99 and sAC were immunoprecipitated from HUVEC whole-cell lysate. Immunoblot analysis was performed for CD99, sAC, PKA-RIIα, ezrin, and AKAP-13. Cell lysates were probed in parallel for loading controls. (d) Endogenous CD99 was immunoprecipitated from iHUVECs expressing either SCR or sAC shRNA. Immunoblot analysis was performed for ezrin, sAC, and CD99 for both cell lysates and immunoprecipitation samples. (e) Quantification of lysates. Efficacy of sAC knockdown was quantified by normalizing sAC expression to CD99. Values were then normalized to the SCR shRNA/CD99 IP condition. (f and g) Quantification of coimmunoprecipitation samples. The amount of sAC (f) and ezrin (g) that coimmunoprecipitated with CD99 was calculated and normalized to the SCR shRNA CD99 IP condition. (h) Endogenous CD99 was immunoprecipitated from iHUVECs expressing either SCR or ezrin shRNA. Immunoblot analysis was performed for ezrin, sAC, and CD99 for both cell lysates and immunoprecipitation samples. (i) Quantification of lysates. Efficacy of ezrin knockdown was quantified by normalizing ezrin expression to CD99. Values were then normalized to the SCR shRNA CD99 IP condition. (j and k) Quantification of coimmunoprecipitations. The amount of sAC (j) and ezrin (k) that coimmunoprecipitated with CD99 was calculated and normalized to the SCR shRNA CD99 IP condition. (l) Quantitative TEM assays were performed using HUVECs pretreated with CD99, ezrin, or SCR shRNA. (m) HUVECs were treated in parallel and used for immunoblot analysis of ezrin, CD99, and β-actin. (n) Quantification of results above. Ezrin and CD99 expression was normalized to β-actin for each condition. Values were then normalized to SCR shRNA conditions. Bars, 10 µm. Images are representative of three (a–d, h, and m) independent experiments. Numerical values are the mean of three (e–g, i–l, and n) independent experiments. Error bars represent SD **, $P < 0.01$; ***, $P < 0.001$; ****, $P < 0.0001$; Student's *t* test [e–g and i–l] and ANOVA [n]).

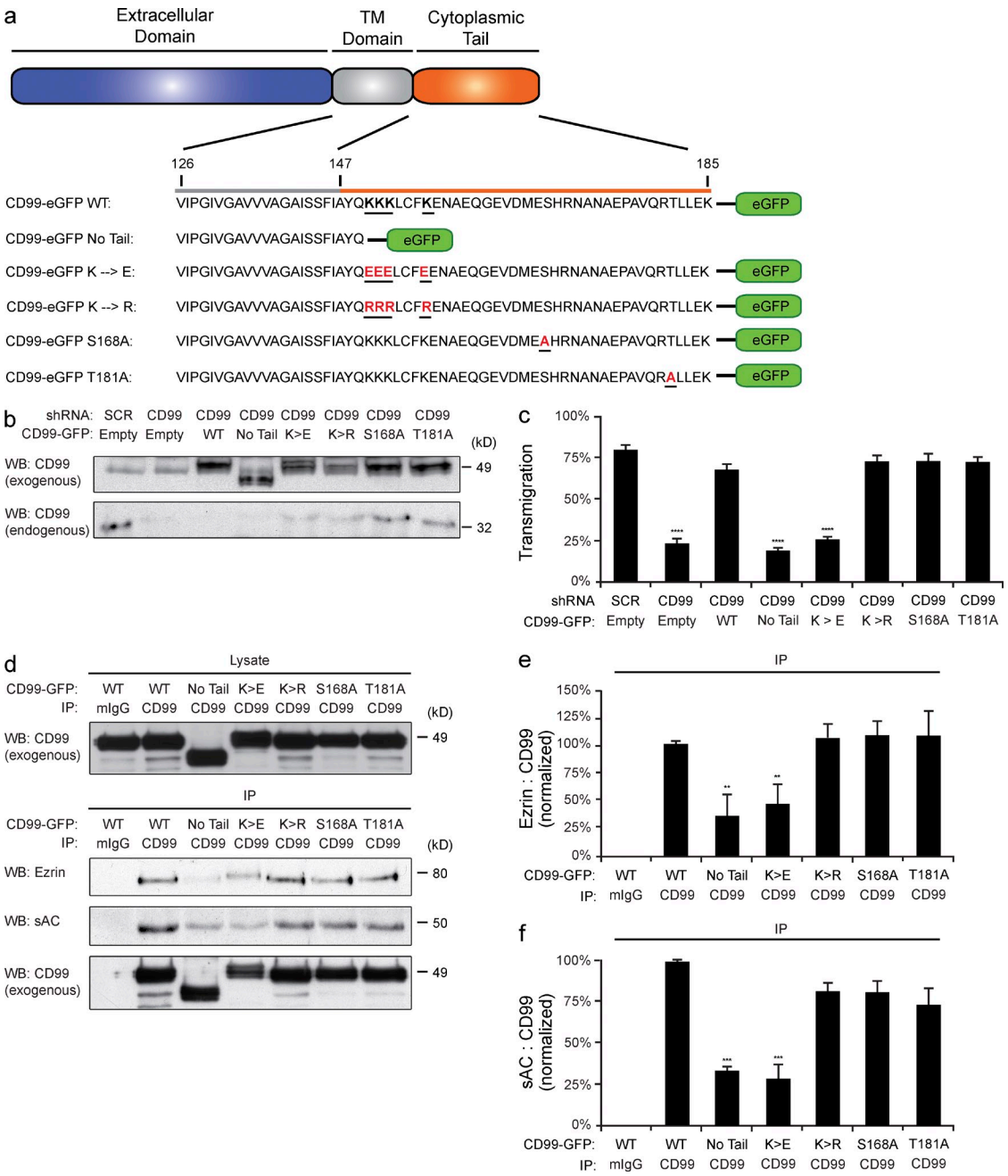

Figure 8. CD99 cytoplasmic tail mediates TEM through a positively charged juxtamembrane region. (a) Diagram of CD99 cytoplasmic tail and CD99-GFP constructs. (b) Endogenous CD99 in HUVECs was knocked down using CD99 shRNA. CD99-GFP constructs were then reexpressed. Samples treated in parallel were lysed and used for immunoblot analysis of CD99 to assess degree of reexpression and knockdown. (c) Quantitative TEM assays were then performed on knockdown samples. (d) CD99-GFP constructs were overexpressed in iHUVECs. CD99 was then immunoprecipitated from the surface of cells (ensuring only fully processed CD99 was being analyzed). Immunoblot analysis for ezrin, sAC, and CD99 was then performed. (e and f) Quantification of results above. Amount of ezrin (e) and sAC (f) in each sample was normalized to the amount of CD99 immunoprecipitated (to account for any variability in pull-down efficiency between samples). Values were then normalized to wild-type CD99-GFP condition. Images are representative three (b and d) independent experiments. Numerical values are the mean of three (c, e, and f) independent experiments. Error bars represent SD (e and f) or SEM (b; ***, $P < 0.001$; ****, $P < 0.0001$; ANOVA).

plasma membrane of HUVECs to avoid complications of any potential trafficking defects caused by our mutations (see Materials and methods). Additionally, CD99–GFP constructs were expressed at roughly 5–10 times that of residual endogenous CD99 (unpublished data). Therefore, the majority of molecules that were immunoprecipitated were the exogenous constructs. Immunoblot analysis revealed that loss of the cytoplasmic tail or loss of the positively charged juxtamembrane

region attenuated the ability of CD99 to interact with sAC and ezrin (Fig. 8, d–f). The small amount of sAC and ezrin seen with these constructs was likely caused by the fraction of endogenous CD99 that was immunoprecipitated. From this, we concluded that the lysine-rich, positively charged juxtamembrane region of the CD99 cytoplasmic tail is critical for its association with sAC and ezrin.

sAC is critical for leukocyte TEM in vivo

CD99 has been shown to be critical for leukocyte transmigration in vivo (Bixel et al., 2004; Dufour et al., 2008; Bixel et al., 2010). To test if sAC is also required for leukocyte extravasation in vivo, we used a model of dermatitis. Before stimulation with croton oil, mice were pretreated with either anti-CD99 (clone 3F11 mAb; Fig. 9 a), KH7, or carrier alone (DMSO). 3D confocal microscopy of fixed tissue revealed that although mice treated with carrier alone showed robust neutrophil influx into the perivascular space of the ear, treatment with either anti-CD99 or KH7 significantly attenuated this response (Fig. 9, b and c). To further identify the step at which anti-CD99 and KH7 were acting to block extravasation, we analyzed xz-orthogonal sections to discern where neutrophils were being arrested (Fig. 9 b, insets). Cells were scored as being in one of six positions (Fig. 9 d). Both anti-CD99 and KH7 arrested the vast majority of leukocytes partway through the endothelial junctions (Fig. 9 e), replicating the phenotype seen upon blocking CD99 or sAC function in vitro. There was no difference in mean vessel length, diameter, or the total number of PMN per field among the groups (unpublished data). Additionally, pretreatment of PMN with KH7 did not affect their ability to transmigrate across endothelial monolayers in vitro (not depicted). Therefore, we conclude that the effect of anti-CD99 and KH7 was on transmigration and not previous steps required for leukocyte requirement.

In vitro, we overcame the block to TEM rendered by anti-CD99 mAb using a H2-R agonist to directly activate PKA (Fig. 2 b). To test this in vivo, we preteated mice with either anti-CD99 or control IgG and stimulated their ears with croton oil. 2 h before harvesting the tissue, we injected dimaprit (10 mg/kg; Bastaki et al., 2008) or carrier alone. As observed in vitro, activation of the H2-R was able to overcome the anti-CD99 blockade of TEM in vivo (Fig. 9, f and g). As a control, mice treated with anti-CD99 were sacrificed at the time dimaprit was given to ensure extravasation was blocked throughout the experiment; there was no difference between these mice and those in the anti-CD99/carrier treatment group (Fig. 9 h). Additionally, when comparing the xz-orthogonal views to assess sites of blockade, we noticed that upon treatment with dimaprit there was a shift from leukocytes being arrested in the middle of endothelial junctions to subsequent steps of extravasation (arrest on the basement membrane or migrating through the basement membrane, Fig. 9 i). This phenomenon could be caused by prematurely stopping the restoration of the anti-CD99 blockade; if we waited longer after giving dimaprit, we might have seen a higher percentage of restoration in the dimaprit-treated anti-CD99 group. Importantly, there was no difference in mean vessel length, diameter, or the total number of PMN per field among the groups (not depicted).

To test the effect of genetic deletion of sAC in ECs, we generated an endothelial-specific sAC knockout by crossing conditional sAC knockout mice (sAC-C2$^{flox/flox}$; Chen et al., 2013) with VE-Cre mice (Alva et al., 2006). Because hemogenic endothelium bears VE-cadherin, there have been reports of variable numbers of leukocytes also being affected by this cre recombinase (Kim et al., 2005b). Therefore, we tested the specificity of the knockout in our hands. At the conclusion of the experiments, we isolated the peripheral blood and heart ECs (MHECs) from the mice used in the experiments below. Cells were then sorted by FACS into two populations: MHECs (CD31$^+$/CD45$^-$) and leukocytes (Ly6G$^+$/CD45$^+$). DNA was extracted from these populations and PCR was performed to assess the expression of the full-length (wild-type) sAC allele and the sAC-C2 knockout allele. The ECs in the VE-Cre$^+$ mice bore the knockout allele, whereas the leukocytes from these mice had almost exclusively wild-type sAC (Fig. 10 a). In addition, we analyzed the expression of ICAM-1 on the postcapillary venules of carrier-treated and croton oil–treated sAC-C2$^{flox/flox}$ and sAC-C2$^{flox/flox}$/VE-Cre$^+$ mice. Deletion of sAC in ECs had no effect on the expression of ICAM-1 under either condition (unpublished data).

The endothelial-specific sAC KO mice were subjected to inflammation in our croton oil dermatitis model. Mice in which endothelial sAC was ablated (sAC-C2$^{flox/flox}$/VE-Cre$^+$) showed significantly attenuated transmigration compared with control mice (sAC-C2$^{flox/flox}$; Fig. 10, b and c). Furthermore, we analyzed where the neutrophils were being arrested in these mice (Fig. 10 b insets) and similar to KH7 and anti-CD99–treated mice, the majority of leukocytes were arrested partway through the endothelium (Fig. 10 d). There was no difference in average vessel length, diameter, or the total number of PMN per field among the groups (not depicted). From these data, we confirm specifically that endothelial sAC is critical for leukocyte extravasation in vivo.

DISCUSSION

Although CD99 has been known to be critical for leukocyte transmigration for over a decade (Schenkel et al., 2002; Bixel et al., 2004, 2010; Lou et al., 2007; Dufour et al., 2008), the mechanism has remained completely unknown. Here, we report that homophilic engagement of endothelial CD99 recruits membrane from the LBRC to sites of leukocyte–endothelial contact to facilitate the passage of leukocytes through the endothelial junctions. This engagement of endothelial CD99 (Fig. 10 e, #1) signals through sAC (Fig. 10 e, #2) to activate PKA (Fig. 1 e, #3), which works through a yet-to-be-defined mechanism (Fig. 10 e, #4) to induce LBRC membrane trafficking (Fig. 10 e, #5). Furthermore, we demonstrate that CD99 and sAC are held together in a signaling complex with ezrin and PKA and that this interaction is dependent on a lysine-rich juxtamembrane region in the cytoplasmic

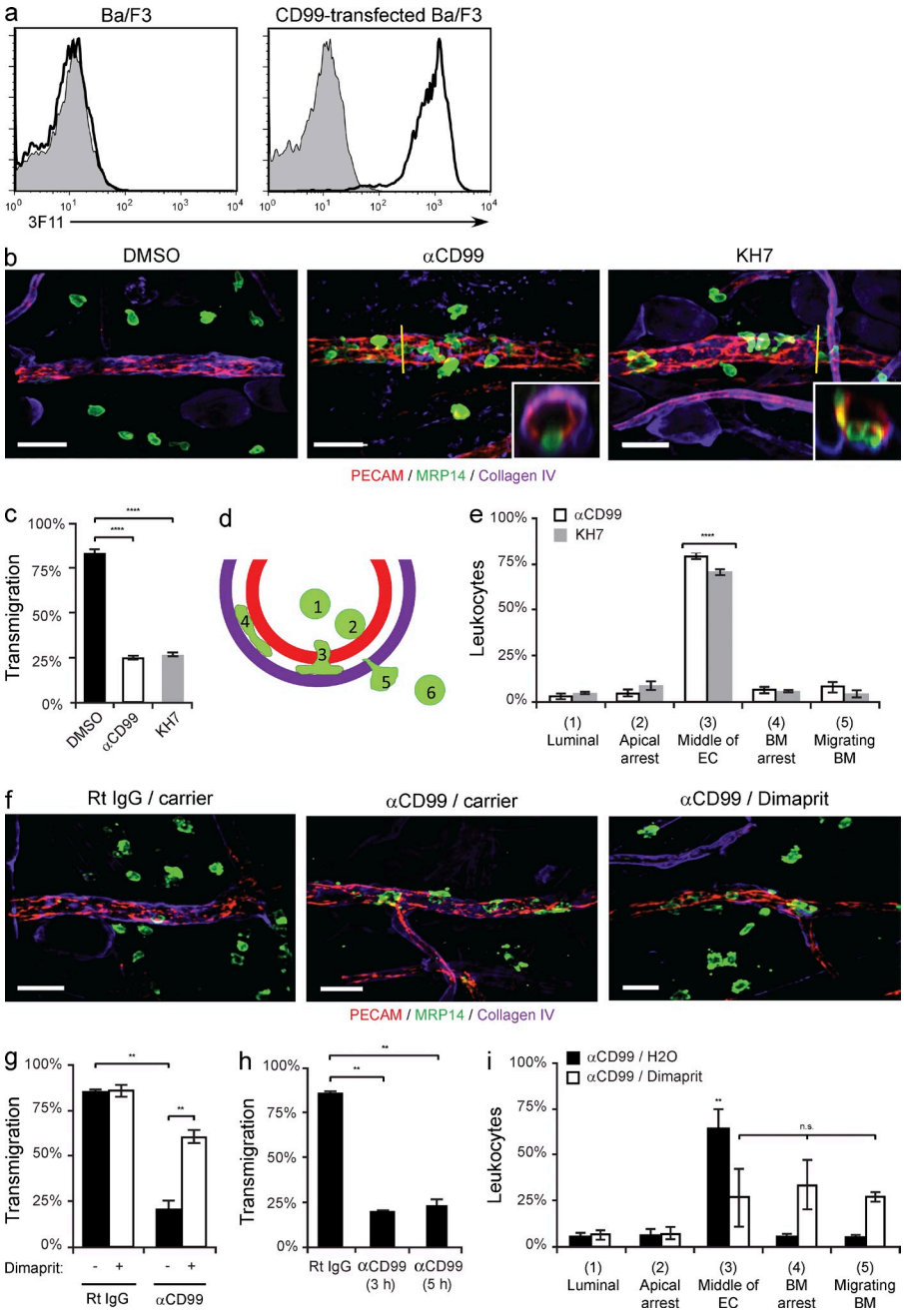

Figure 9. SAC is critical for leukocyte transmigration in vivo. (a) Validation of rat anti–mouse CD99 monoclonal antibody, clone 3F11. Flow cytometry analysis of control (shaded) or anti–mouse CD99 (3F11, thick line) mAb binding to parental or mouse CD99-transfected Ba/F3 cells. (b) The ears of wild-type FVB/n mice (age and sex matched littermates) pretreated with DMSO, anti-CD99 (3F11 mAb), or KH7 (5 µmol/kg) were stimulated with croton oil (1%, 20 µl/ear) or carrier (10% olive oil/90% acetone). After 5 h, mice were sacrificed, their ears were harvested, and immunohistochemical staining was performed using anti-PECAM (ECs), anti-MRP14 (neutrophils), and anti–collagen-IV (basement membrane). 3D confocal images were acquired for each sample. (c) Quantification of results above. Percent of leukocytes extravasated within 50 µm of venules per field of view. (d) Model for quantification of site of arrest. Neutrophils were scored as being in one of six positions: luminal (1), apically arrested (2), arrested partway through the endothelium (3), arrested on the basement membrane (4), migrating through the basement membrane (5), or fully extravasated (6). (e) Quantification of the site of arrest for anti-CD99 and KH7-treated animals. (f) The ears of wild-type FVB/n mice (age- and sex-matched littermates) pretreated with anti-CD99 or rat IgG (control) were stimulated with croton oil. After 3 h, mice received dimaprit (10 mg drug/kg animal) or carrier (H_2O). Mice were sacrificed 2 h later, their tissue stained, and analyzed as described in panel b. (g) Quantification of results. Percent of leukocytes extravasated within 50 µm of venules per field of view. (h) Additional mice pretreated with anti-CD99 mAb were sacrificed at the time dimaprit was given (3 h) to ensure that the anti-CD99 blockade was present throughout the experiments (5 h total). (i) Quantification of the site of arrest for anti-CD99/carrier and anti-CD99/dimaprit-treated animals. 100–200 cells were analyzed per ear. Total PMN per field of view, vessel length, and vessel diameter were equivalent for all conditions tested (not depicted). Images were acquired with a 40× objective (n = 1.00). Insets show xz-orthogonal view (where yellow bar dissects the vessel) to demonstrate site of neutrophil arrest. Bars, 25 µm. Two to three mice per condition were used for each experiment. Images are representative of two (f) or three (a and b) independent experiments. Data represent the average value of two (g-i) or three (c and e) independent experiments. Error bars denote SEM ***, $P < 0.001$; ****, $P < 0.0001$; Student's t test [c and g] and ANOVA [e and i]).

tail of CD99. These findings represent the first description of the immediate downstream signaling mechanisms of CD99, as well as the first demonstration of a role for sAC in leukocyte TEM.

There are parallels between our findings on LBRC trafficking and other membrane movement in physiology. In gastric parietal cells, PKA activation by the H2 receptor results in massive flux of tubulovesicle membrane to the apical secretory surface (Forte and Zhu, 2010). Ezrin has been shown to be critical for promoting this membrane movement, linking the gastric apical cAMP microdomain with the actin cytoskeleton. We found in this study that CD99 functions locally to activate PKA and promote the movement of LBRC. Furthermore, ezrin appears to be critical to the function of CD99, as well; it localizes sAC to the cytoplasmic tail of CD99 so that it can activate PKA. As with parietal cell physiology, the downstream

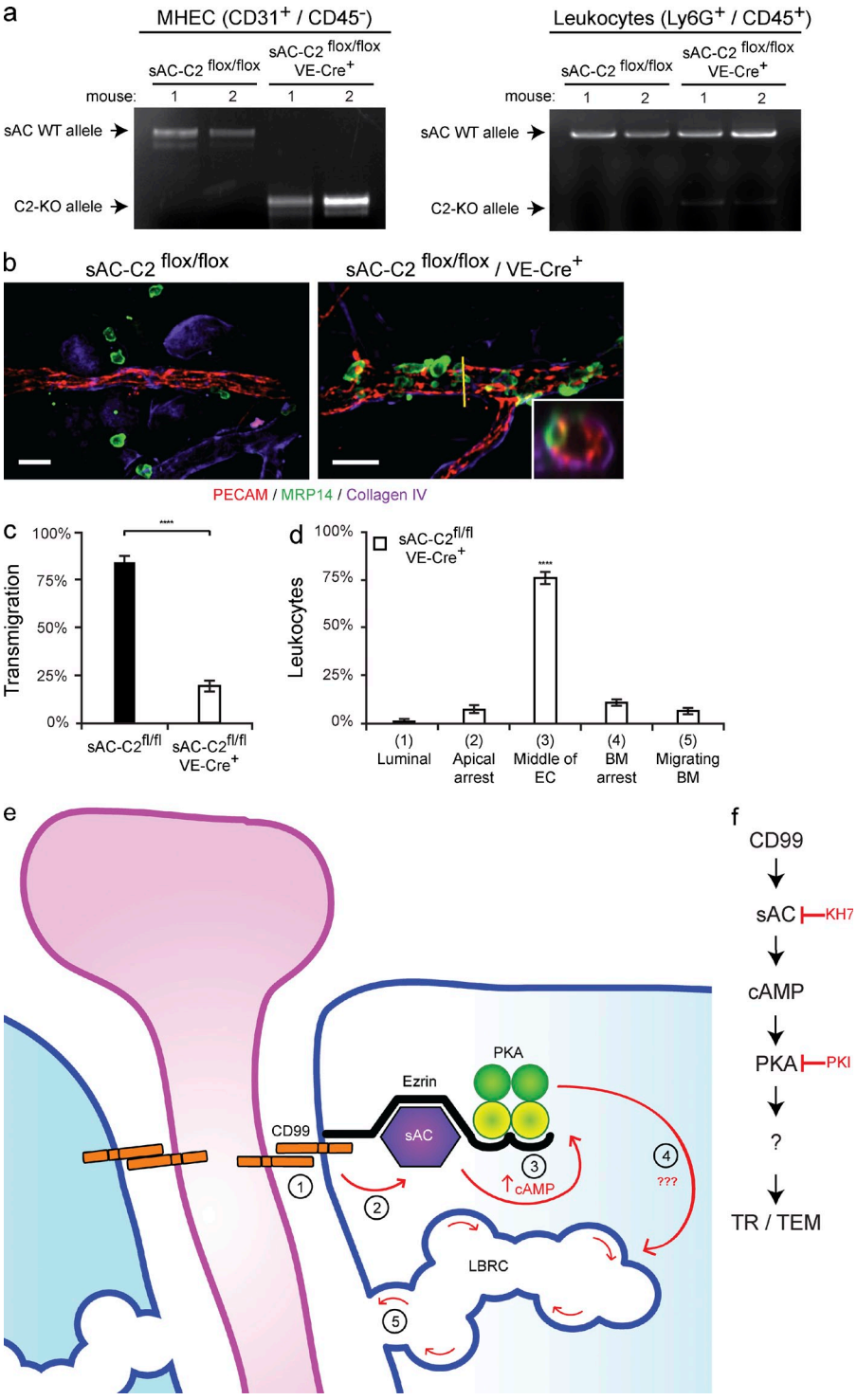

Figure 10. Endothelial-specific knockout of sAC blocks leukocyte transmigration in vivo. (a) Heart tissue and peripheral blood was collected from sAC-C2$^{flox/flox}$ and sAC-C2$^{flox/flox}$/VE-Cre^{+} mice used in the following experiments (see Materials and methods). FACS was used to sort MHEC (CD31^{+}/CD45^{-}) and leukocyte (Ly6G^{+}/CD45^{+}) cell populations from the heart tissue and peripheral blood, respectively. MHEC and leukocyte DNA was isolated from each mouse. PCR was performed to assess the expression of either sAC WT allele (top band) or sAC C2-KO allele (bottom band). (b) The ears of sAC-C2$^{flox/flox}$ or sAC-c2$^{flox/flox}$/VE-Cre^{+} mice (mixed background, see Materials and methods; Chen et al., 2013) were stimulated for 5 h with croton oil. Tissue was then harvested, stained, and analyzed. (c) Quantification of results above. (d) Quantification of site of arrest for sAC-C2$^{flox/flox}$/VE-Cre^{+} mice. Percent of leukocytes extravasated within 50 µm of venule per field of view. (e) Our current model of how CD99 signals during TEM. Under resting conditions, CD99, sAC, PKA, and ezrin form a signaling complex at endothelial junctions. During TEM, homophilic engagement of endothelial CD99 with leukocyte CD99 (#1) signals through sAC (#2) to elevate cAMP (#3), to activate PKA, which works through a yet to be defined mechanism (#4) to induce LBRC membrane trafficking to sites of leukocyte–endothelial contact (#5). (f) Flow diagram of model detailed above. 100–200 cells were analyzed per ear. PMN per field of view, vessel length and vessel diameter were equivalent for all conditions tested (not depicted). Images were acquired with a 40× objective (n = 1.00). Insets show xz-orthogonal view (where yellow bar dissects the vessel) to demonstrate site of neutrophil arrest. Bars, 25 µm. Three mice per condition were used for each experiment. Images are representative of three (a and b) independent experiments. Data represent the average value of three (c and d) independent experiments. Error bars denote SEM (****, $P < 0.0001$; Student's t test [c] and ANOVA [d]).

targets of PKA that link its activation to the trafficking of intracellular membrane are not known. However, this is an area of future interest.

cAMP is an abundant second messenger for numerous, often concurrent, cellular processes. It is critical that its activity be tightly regulated and localized to discrete microdomains within the cell to ensure precise spatiotemporal signaling (Zaccolo M, 2009). Approximately 50 AKAPs have been identified in different cell types to date in Jarnaess and Taskén, (2007); however, little is known about the AKAP expression profile in EC. Ezrin is also a member of the ERM (ezrin/radixin/moesin) family, a group of proteins that link the plasma membrane to the actin cytoskeleton. Actin remodeling during leukocyte TEM is a dynamic process that requires

rapid signaling between adhesion molecules and actin effector molecules (Alcaide et al., 2009; van Buul and Hordijk, 2009). We demonstrate that ezrin interacts with CD99 through a positively charged juxtamembrane region in its cytoplasmic tail. This raises the possibility that CD99 signaling could directly affect actin remodeling during leukocyte transmigration; a possibility that is currently being investigated.

cAMP-induced activation of Rap1, through Epac, stabilizes VE-cadherin at cell–cell junctions and decreases barrier permeability (Fukuhra et al., 2006; Noda et al., 2010). Although this function of cAMP may seem to contradict its role in CD99 signaling, it is important to note that vascular permeability and leukocyte TEM are molecularly distinct events; increased permeability can occur with decreased leukocyte extravasation (Schnoor et al., 2011). We demonstrate here (Fig. 3 f) that only cAMP capable of activating PKA is able to restore the anti-CD99 blockade of TEM; an EPAC-selective cAMP analogue has no effect. Therefore, it is likely that the pool of intracellular cAMP generated upon engagement of CD99 is localized specifically near the cytoplasmic tail of CD99 and is separate from the pool regulating VE-cadherin dynamics.

SAC is encoded by a single gene containing >30 exons. However, multiple promoters and extensive alternative splicing yield a variety of isoforms (Jaiswal and Conti, 2001; Geng et al., 2005; Farrell et al., 2008). Full-length sAC (sAC_{fl}) represents the entire 187-kD protein, whereas the minimal functional variant sAC_t, is a truncated form (50 kD) consisting of the two C terminus catalytic domains. sAC_t has been implicated in a variety of cellular functions, including renal epithelial physiology (Tresguerres et al., 2011). Similar to epithelial cells, where sAC_t appears to be enriched at apical and basolateral membranes (Paunescu et al., 2008), we observed a distinct subset of sAC_t-GFP at sites of EC–cell contact, colocalizing with the junctional adhesion molecule CD99. Additionally, in HUVECs, the predominant form of sAC that coimmunoprecipitated with CD99 is ∼50 kD. Upon treatment with sAC shRNA, the 50-kD sAC isoform was significantly knocked down, correlating with a decrease in leukocyte transmigration, and reexpression of rat sAC_t–rescued TEM (Fig. 7). These data suggest that sAC_t is the isoform of sAC that interacts with CD99 to regulate diapedesis. Our work identifies sAC as a key regulator of leukocyte extravasation, and therefore a potential therapeutic target for treating inflammatory disease.

Although CD99 has been shown to function downstream of PECAM during diapedesis in vitro (Schenkel et al., 2002; Lou et al., 2007; Sullivan et al., 2013), the step at which CD99 functions in transmigration in vivo has not been as well defined (Bixel et al., 2004, 2010; Dufour et al., 2008). In our current study, we demonstrate that when CD99 function is blocked in vivo, neutrophils are indeed arrested partway across the endothelial lining, as they are in vitro (Fig. 9). Bixel et al. (2010) reported that blocking CD99 using a polyclonal antibody arrested neutrophils between the endothelium and the basement membrane in the cremaster circulation. The difference between these observations could be due to several important variables, including differences in mouse strain (Schenkel et al., 2004; Seidman et al., 2009), vascular bed, or the confocal resolution of the xz-plane. This last point is especially important as z-axis resolution is the ultimate limitation of microscopy and critical for the conclusions drawn in these experiments (see Materials and methods for information on the microscope used in these studies). However, to definitively discern where CD99 is functioning in relation to the endothelium, this process should be studied in real time, in vivo, comparing the two strains head to head, a study that is currently underway in our laboratory.

In conclusion, CD99, sAC, and PKA are tethered by ezrin to EC junctions. Engagement of EC CD99 activates sAC, which stimulates PKA and induces continued recruitment of membrane from the LBRC to sites of transmigration to facilitate diapedesis.

MATERIALS AND METHODS

Procedures. All procedures involving human subjects and human materials were approved by the Institutional Review Board of Northwestern University Feinberg School of Medicine.

Antibodies and reagents. Mouse IgG_{2a} anti–human PECAM (clone hec7; Muller et al., 1989), mouse IgG_{2a} anti–human VE-cadherin (clone hec1; Ali et al., 1997), mouse IgG_1 anti–human CD99 [hec2]; Schenkel et al., 2002), mouse IgG_{2a} anti–human CD18 (clone IB4; Wright et al., 1983), and Armenian hamster anti–mouse PECAM (clone 2H8; Schenkel et al., 2004) were produced in the laboratory via hybridoma methodologies. The nonfunctional blocking mouse anti–human PECAM antibody (clone P1.1; Liao et al., 1995) was purified from mouse ascities fluid from P. Newman (Blood Center of Wisconsin, Milwaukee, WI) according to standard methods. Mouse IgG_1 anti–human sAC (clone R21), biotinylated R21, and mouse IgG_{2b} anti–human sAC (clone R37) were generated as previously described (Buck et al., 1999; Farrell et al., 2008). Rabbit anti–human ADCY10, rabbit anti–human β-actin, rabbit anti–mouse collagen IV, rat anti–mouse MRP-14, and rabbit anti–human AKAP13 were purchased from Abcam. Rabbit anti–human phospho PKA Thr197, rabbit anti–human PKA Cα, rabbit anti–human phospho-VASP Ser157, rabbit anti–human VASP (clone 9A2), rabbit anti–human phospho-CREB Ser133 (clone 87G3), rabbit anti–human CREB (clone 48H2), and rabbit anti–human ezrin were purchased from Cell Signaling Technology. Rabbit anti–human CD99, rabbit anti–human PKA-RIIα, and mouse anti–human ezrin (clone 3C12) were purchased from Santa Cruz Biotechnology, Inc. Rabbit anti–human CD54 (ICAM-1) was purchased from AbD Serotec. PE rat anti–mouse Ly6G, PE Rat IgG2a, FITC rat anti–mouse CD31, FITC Rat IgG2b, APC rat anti–mouse CD45, and APC Rat IgG2b were purchased from BioLegend. Nonspecific mouse IgG_1, GαM IgG_1, GαM IgG_{2a}, goat anti–rabbit IgG, goat anti–Armenian hamster IgG, Alexa Fluor 488 goat anti–rat IgG, and Alexa Fluor 647 donkey anti–rabbit IgG were purchased from Jackson ImmunoResearch Laboratories. DyLight-488 and -550 GαM IgG2a and DyLight-550 goat anti–Armenian hamster were conjugated using a kit purchased from Thermo Fisher Scientific.

Forskolin, 8-(4-Chlorophenylthio) adenosine 3′,5′-cyclic monophosphate, ddAdo, histamine dihydrochloride, diphenhydramine hydrochloride, ranitidine hydrochloride, JNJ 10191584 maleate salt, and dimaprit dihydrochloride were purchased from Sigma-Aldrich. KH7 was purchased from Cayman Chemical Company. PKI_{14-22} myristolyated amide and 8-pCPT-2-O-Me-cAMP-AM were purchased from Tocris Bioscience. Recombinant human TNF was purchased from R&D Systems.

Isolation and culture of human ECs. Human umbilical vein ECs (HUVECs) were isolated from human umbilical cords as previously described (Muller et al., 1989; Muller and Luscinskas, 2008). At their second passage,

HUVECs were cultured on three-dimensional type-I collagen matrices (PureCol; Inamed Biomaterials) to ensure formation of high-quality basement membranes (Muller et al., 1989; Muller and Luscinskas, 2008). For adenoviral infection, HUVECs were infected for 72 h for shRNA adenoviruses and 48 h for rescue and GFP constructs.

Immortalized HUVECs (iHUVECs) were generated and grown as previously described (Ancuta et al., 2003; Yang et al., 2005). In brief, this line was generated from HUVECs transduced with LSNX-16E6E7 retrovirus (encoding HPV-16 oncoproteins E6 and E7). These cells have been shown to express similar levels of adhesion molecules and to support TEM similarly to unmodified HUVECs (Ancuta et al., 2003; Yang et al., 2005; Feng et al., 2015).

Isolation of human peripheral blood mononuclear leukocytes (PBMCs). PBMCs were isolated as previously described (Muller and Weigl, 1992; Muller and Luscinskas, 2008). In brief, blood was drawn from healthy volunteers into 1/10 volume EDTA (10 mmol/l) and mixed with an equal volume of HBSS (Mediatech Inc.). Blood/HBSS mixture was layered over Ficoll-Paque density gradient medium (GE Healthcare) and centrifuged at 2,200 rpm for 20 min. The upper plasma layer was collected. The PBMC layer was collected and diluted in HBSS. Both PBMC and plasma were centrifuged at 1,500 rpm for 10 min. The PBMC pellet was resuspended in the spun platelet-depleted plasma and centrifuged at 1,200 rpm for 5 min. The resulting PBMC pellet was washed 3 times with HBSS via resuspension and centrifugation at 1,200 rpm for 5 min. The final PBMC pellet was resuspended in M199 (Invitrogen) containing 0.1% human serum albumin (HSA; Grifols Biological Inc.).

Isolation of human polymorphonuclear cells (PMNs). PBMC were isolated as previously described (Lou et al., 2007). In brief, blood was drawn from healthy volunteers into 1/10 volume EDTA (10 mmol/l). Blood/EDTA mixture was layered over PolymorphPrep gradient medium (Axis-Shield) and centrifuged at 1,800 rpm for 30 min. The PMN layer was collected, diluted in room temperature HBSS/HAS, and centrifuged at 750 rpm for 5 min. The PBMC pellet was resuspended in HBSS/HSA, counted, and centrifuged at 750 rpm for 5 min once more. The final PMN pellet was resuspended in M199 (Invitrogen) containing 0.1% HAS (Grifols Biological Inc.).

Isolation of MHECs and mouse peripheral blood leukocytes. MHECs were isolated as previously described (Lim et al., 2003). In brief, hearts were dissected from 6–8-wk-old mice after experiments. Tissue was then dissociated using Type-II Collagenase (Life Sciences). RBCs were lysed using Pharm Lysis Buffer (BD). Tissue homogenate was labeled and sorted by FACS.

Mouse leukocytes were isolated from peripheral blood. In brief, blood was collected via facial vein puncture. RBCs were lysed. Cells were then labeled and sorted by FACS.

Mouse strains. FVB/n wild type mice were originally purchased from The Jackson Laboratory (JAXE). sAC-C2 floxed mice (mixed background; Chen et al., 2013) were crossed with VE-Cre mice (C57BL/6 background; Alva et al., 2006) to generate sAC-C2 endothelial-specific knockout mice. All mice were raised and housed at Northwestern University Feinberg School of Medicine (Chicago, IL). All procedures were approved by the Institutional Animal Care and Use Committee of Northwestern University.

Cloning of shRNA, CD99, sAC, and ezrin adenoviral constructs. CD99 shRNA (5′-GGCTGGCCATTATTAAGTCT*TCAAGA*GAGACTTAATAATGGCCAGCCTTTTT-3′) and scrambled control (SCR, 5′-ACTACCGTTGTTATAGGTGT*TCAAGA*GACACCTATAACAACGGTAGTTTTTT-3′) were generously provided in the pSilencer2.1 vector by K. Scotlandi (Rizzoli Orthopedic Institute, Bologna, Italy). sAC shRNA (sACsh1, 5′-CCGGCCGTACTGAGAAAGTCATGTT*CTCGA*GAACATGACTTTCTCAGTACGGTTTTT-3′, sACsh2, 5′-CCGGGCTCAGATGAATGATGTTATTC*TCGA*GAATAACATCATTCATCTGAGCTTTTT-3′) were purchased from Sigma-Aldrich in the pLKO.1 vector. Ezrin shRNA sequences were created from previously published siRNA sequences (Osawa et al., 2009; ezrin1 shRNA, 5′-AAGCTGGATAAGAAGGTGTCT*TCGA*AGACACCTTCTTATCCAGCTT-3′; ezrin2 shRNA, 5′-AAGGAATCCTTAGCGATGAGA*TCGA*TCTCATCGCTAAGGATTCCTT-3′). The shRNA constructs and hU6 promoters were cloned into the pENTR4 plasmid (Invitrogen). These vectors were recombined with the adenoviral vector pAd/PL-DEST (Invitrogen) using LR Clonase (Invitrogen) according to the manufacturer's guidelines and used to produce adenovirus for transduction according to standard methods (Zhang et al., 2006).

The full-length CD99-GFP construct and its pCMV promoter were cloned into the pENTR4 vector. Site-directed mutagenesis was then performed to generate the CD99-GFP cytoplasmic tail mutants. These constructs were subsequently recombined with the pAd/PL-DEST plasmid to produce adenovirus.

Rat sAC_t was originally supplied in the pDEST26 vector (Invitrogen). Rat sAC_t and its pCMV promoter were cloned into the pENTR4 plasmid. Site-directed mutagenesis was used to induce two silent mutations in the sAC_t cDNA rendering it resistant to sAC shRNA-1 and -2. To generate sAC_t-GFP, sAC_t was inserted in frame with eGFP in the pENTR4 vector, encoding a C-terminal eGFP linked fusion protein. These constructs were then recombined with pAd/PL-DEST and used to produce adenovirus.

For adenoviral infection of HUVECs, cells were seeded either on three-dimensional collagen matrices (96-well) or fibronectin-coated tissue culture surfaces (6-well). The following day, monolayers were washed 3 times with serum-free M199 and incubated with shRNA adenovirus for 24 h. The next day, cells were wash three times and incubated with rescue construct or GFP construct adenovirus. The following day, cells were washed and incubated with fresh media for 24 h before being used in experiments. With this protocol, the knockdown and reexpression constructs were expressed for 72 and 48 h, respectively.

Generation of anti–mouse CD99 monoclonal antibody. Wistar rats (SLC) were immunized with mouse CD99-Fc fusion protein (Wang et al., 2013) using TiterMax Gold (TiterMax) as an adjuvant. 2 wk after immunization, lymph node cells were fused with SP2/0, and a clone that recognized mouse CD99-transfected Ba/F3 cells was obtained (clone 3F11; Fig. S7). The mAb produced in culture supernatant was purified by protein G affinity chromatography (GE Healthcare).

Protein cross-linking. Confluent, resting HUVECs were incubated with anti-CD99 (clone hec2), anti-PECAM (clone hec7), or $mIgG_1$ for 1 h at 37°C. Cells were then washed to remove nonbound mAb and subsequently incubated with GαM secondary antibodies for 10 min at 37°C. The HUVECs were then lysed immediately in boiling sample buffer. Where indicated cells were pretreated with the following inhibitors: PKI (5 μM, 1 h), KH7 (50 μM, 1 h), and ddAdo (25 μM, 1 h) before cross-linking for the indicated times.

Polystyrene microsphere (bead) coating. Polystyrene microspheres were coated as previously described (Sullivan et al., 2013). In brief, amino-functionalized polystyrene beads (Polysciences; 3 μm) were washed and resuspended in 8% glutaraldehyde in PBS for 2 h at room temperature. Beads were washed and incubated with 200 μg/ml of anti-CD99 mAb, anti-PECAM mAb, or control $mIgG_1$ for 2 h at room temperature. Beads were then washed and blocked with 0.1 M Glycine in PBS for 2 h at RT. Conjugate beads were washed once more and stored in PBS for up to 1 wk without noticeable loss of efficacy.

For bead recruitment experiments, HUVEC monolayers were grown on fibronectin-coated dishes (MatTek Corporation) and transduced for 48 h with wild-type CD99-GFP adenovirus. The day of the experiments, beads were washed, diluted in preconditioned HUVEC media, and added to dishes. Beads were allowed to settle and bind for 20 min at 37°C. Monolayers were then washed with PBS and fixed with 4% paraformaldehyde. Monolayers were subsequently permeabilized and stained for VE-cadherin and phospho-PKA Thr197. All images within each experiment were captured under identical settings and processed in parallel with ImageJ (National Institutes of Health) to preserve relative intensities in immunofluorescence staining.

Immunofluorescence microscopy. Confluent HUVECs were washed with PBS and fixed in 4% paraformaldehyde for 10 min at 37°C. Cells were then washed 3 times and permeabilized with 0.1% Triton-X 100 for 10 min at room temperature. Blocking buffer (PBS with 2.5% BSA; Sigma-Aldrich; 2.5% host species serum; Jackson ImmunoResearch Laboratories) was added for 1 h at room temperature. Cells were then incubated with primary antibody at 10 μg/ml in blocking buffer overnight at 4°C. VE-cadherin was detected by hec1. Phosphorylated PKA was detected by pPKA Thr197 (Cell Signaling Technology). The next day, cells were incubated with secondary antibody (DyLight-550 GαM IgG_{2a}, Alexa Fluor 647 goat anti–rabbit; Jackson ImmunoResearch Laboratories) for 1 h at room temperature in PBS. Confocal images were visualized using an Ultraview Vox imaging system equipped with a Yokogawa CSU-1 spinning disk. Images were acquired with a 40× oil immersion objective using Volocity software (Perkin Elmer).

For immunofluorescence staining of transendothelial migration assays (TEM-IF), after the TEM assay (see TEM assay section) cells were fixed with 4% paraformaldehyde and blocked in blocking buffer as described above. Leukocytes were labeled with DyLight-488–conjugated mouse anti–human CD18 (clone IB4) and HUVECs were labeled with DyLight-550–conjugated mouse anti–human VE-cadherin (clone hec1). Samples were imaged and processed as described above.

Immunoprecipitation and Western blotting. For immunoprecipitation assays, HUVECs were grown to confluency on fibronectin-coated 6-well plates. Cells were washed once with ice cold PBS and lysed in lysis buffer containing 20 mM Tris-HCl, pH 8.0, 137 mM NaCl, 2 mM EDTA, 1% NP-40, 10% Glycerol, 1 mM Na_3VO_4 (New England Biolabs), 1 mM PMSF (Sigma-Aldrich), PhosSTOP phosphatase inhibitor cocktail (Roche), and cOmplete Mini protease inhibitor cocktail (Roche). Lysates were collected and centrifuged at 14,000 rpm for 30 min at 4°C. Supernatants were recovered and precleared with recombinant Protein G–agarose beads (Invitrogen) for 1 h at 4°C with end-over-end rotation. Lysates were then incubated with either mouse anti–human CD99 (clone hec2), mouse anti–human sAC (clone R37), or control mouse IgG_1 for 4 h at 4°C. Immunocomplexes were incubated with Protein G beads for 1 h at 4°C and washed 4–5 times (5–10 min, 4°C) before being resuspended in 2× Laemlli loading buffer with β-mercaptoethanol. The samples were heated at 95°C for 5 min and analyzed by SDS-PAGE. Total cell lysates or immunoprecipitated material were separated by 10% SDS-PAGE and transferred to PVDF (Sigma-Aldrich). Standard Western blotting techniques were then performed to detect desired protein levels. For western analysis of hec2 and R37 immunoprecipitation samples, CD99 levels were detected using rabbit anti–human CD99 (Santa Cruz Biotechnology, Inc.); sAC levels were detected using either biotinylated mouse anti–human sAC (R21B) or rabbit anti–human ADCY10 (Abcam); and ezrin was detected using mouse anti–human ezrin (clone 3C12; Santa Cruz Biotechnology, Inc.).

For immunoprecipitation of CD99-GFP constructs, to ensure only properly processed molecules that had successfully been trafficked to the cell membrane were being analyzed, infected iHUVECs were incubated with either mouse anti–human CD99 (clone hec2) or control mouse IgG_1 for 1 h at 37°C. As hec2 binds to the extracellular domain of CD99, the antibody–antigen complexes can form at 37°C. Cells were washed once in ice-cold PBS and lysed in lysis buffer (see above). Lysates were collected and centrifuged at 14,000 rpm for 30 min at 4°C. Supernatants were recovered and incubated with recombinant Protein G–agarose beads (Invitrogen) for 4 h at 4°C with end over end rotation. Immunocomplexes and beads were washed 4–5 times before being resuspended in 2× Laemlli buffer with β-mercaptoethanol. The samples were heated at 95°C for 5 min and analyzed by SDS-PAGE.

For immunoblot analysis of cross-linked or adenovirus-transduced samples, HUVECs were pretreated as described above and lysed directly into boiling 2× Laemlli loading buffer. Samples were sonicated, incubated at 95°C for 5 min, and analyzed by SDS-PAGE.

TEM assay. TEM assays were performed as previously described (Muller et al., 1989; Muller and Luscinskas, 2008). In this assay, PBMCs are added to resting HUVEC monolayers, but only monocytes transmigrate to any measurable degree over the time course (1 h) of the assay. Similar results are seen using HUVEC monolayers activated by cytokines TNF or IL-1β. PECAM and CD99 are constitutively expressed at endothelial borders; treatment with proinflammatory cytokines TNF or IL-1β does not change their expression levels or distribution (Schenkel et al., 2002). The requirements and mechanisms of TR of leukocytes are the same for neutrophils, monocytes, and lymphocytes under resting or cytokine-activated conditions (Mamdouh et al., 2008). Therefore, most of these studies were performed on monocytes on resting EC monolayers. However, critical results were confirmed with both monocytes and neutrophils on TNF-activated HUVECs. In brief, PBMCs (2×10^6 cells/ml) were added onto confluent HUVEC monolayers grown on hydrated type-I collagen gels and allowed to migrate for 1 h at 37°C. The monolayers were washed twice with 1 mM EDTA in PBS (no Ca^{2+} or Mg^{2+}) and then twice with PBS (with Ca^{2+} or Mg^{2+}) before being fixed in 1% glutaraldehyde in 0.1 M sodium cacodylate buffer (Electron Microscopy Sciences). Fixed cells were stained with modified Wright-Giemsa stain (Protocol Hema3; Thermo Fisher Scientific) and mounted on glass slides. For each sample, at least 100 cells per monolayer were counted using a Zeiss Ultraphot microscope with Nomarksi optics and a SPOT Insight Color CCD (Diagnostic Instruments Inc.). Cells were counted according to their position to the HUVEC monolayer as either above or below the focal plane of the EC nuclei.

For TEM assays in which ECs were treated with blocking antibody, before the addition of PBMC, HUVECs were preincubated with anti-CD99 (clone hec2), anti-PECAM (clone hec7) or anti–VE-cadherin (clone hec1) at 20 μg/ml in preconditioned media for 1 h at 37°C. In TEM assays where ECs were treated with various inhibitors, before the addition of PBMCs, HUVECs were preincubated with the following inhibitors in preconditioned media for 1 h at 37°C: PKI (5 μM PKA inhibitor; Tocris), KH7 (50 μM sAC inhibitor; Cayman Chemical Co.), 2′,5′-dideoxyadenosine (ddAdo; 25 μM tmAC inhibitor; Sigma-Aldrich), diphenhydramine (10 μM H1-R antagonist; Sigma-Aldrich), ranitidine (10 μM H2-R antagonist; Sigma-Aldrich), or JNJ-10191584 (10 μM H4-R antagonist; Sigma-Aldrich) or DMSO (carrier control). HUVECs were then washed extensively in warm PBS before addition of leukocytes. For TEM in which ECs were treated with shRNA adenoviral constructs, HUVECs were infected with shRNA or rescue constructs for 72 and 48 h, respectively, as described above.

In TEM assays in which compounds were briefly added in an attempt to overcome TEM, PBMC were added to HUVEC monolayers and allowed to migrate for 50 min at 37°C. Before washing and fixation, reagents were added at the following working concentrations to the monolayers and cells were incubated for an additional 10 min at 37°C: GαM IgG_1, goat anti–rabbit, 8-CPT (30 μM; Sigma-Aldrich), Forskolin (30 μM; Sigma-Aldrich), histamine (10 μM; Sigma-Aldrich), dimaprit (H2-R agonist; 10 μM; Sigma-Aldrich), 007-AM (3 μM; Tocris) or DMSO (control).

For TEM assays using TNF-activated monolayers, HUVECs were incubated for 4–6 h with recombinant human TNF (R&D Systems) in conditioned media. For experiments using neutrophils, primary human PMNs were isolated (as described above) and added to pretreated HUVEC monolayers. PMNs were allowed to transmigrate for 10 min at 37°C before being washed, fixed, and subsequently analyzed.

TR assay. TR assays were performed as previously described (Mamdouh et al., 2003; Mamdouh et al., 2008). In brief, HUVECs monolayers were grown to confluency on hydrated type 1 collagen gels. Cells were incubated with nonblocking PECAM Fab IgG_{2a} (clone P1.1), as well as function-blocking anti-CD99 IgG_1 (20 μg/ml) or mouse IgG_1 control in preconditioned media for 1 h at 37°C. Monolayers were subsequently washed, chilled, and incubated with a saturating amount (100 μg/ml) of nonconjugated GαM IgG_{2a} (Jackson ImmunoResearch Laboratories) for 1 h at 4°C to bind surface anti-PECAM antibody. After extensive washing of unbound antibody, PBMC (2×10^6 cells/ml) were added to monolayers along with DyLight-550 GαM IgG2a in M199. Cells were kept on ice at 4°C for 15 min to allow PBMC to settle before being warmed at 37°C for 10 min. Cells were subsequently washed and fixed in 4% paraformaldehyde for 10 min at

37°C. Fixed samples were stained with Alexa Fluor 647 anti-CD18 (clone IB4) and imaged using 3-D confocal microscopy. For each sample at least 100 cells per monolayer were counted according to their position relative to endothelial junctions, whether or not they have initiated TEM (as determined by xz-orthogonal view) and whether or not there is enrichment PECAM-bearing membrane around the migrating cells. To quantitate the degree of LBRC enrichment, the mean fluorescence intensity of PECAM staining around leukocytes was measured and divided by the mean fluorescence intensity of PECAM staining of endothelial junctions of the same cell, not in contact with leukocytes.

For experiments in which two antibodies were used to label PECAM recycling, after cells were warmed up at 37°C for 10 min in the presence of DyLight-550 GαM IgG_{2a}, samples were quickly chilled and washed extensively on ice at 4°C. DyLight-488 GαM IgG_{2a} in M199 was then added and cells were kept on ice at 4°C for 15 min. Samples were then warmed to 37°C for 0, 5, or 10 min before being washed, fixed, and stained as described above. The degree of LBRC enrichment (as described above) was quantified for both antibodies over identical portions of the endothelium. Values were calculated for all time points collected.

For restoration experiments, before incubation at 37°C with DyLight 488 GαM IgG_{2a}, 8-CPT (30 μM; Sigma-Aldrich), Forskolin (30 μM; Sigma-Aldrich), or DMSO was quickly added to cells. Samples were then warmed at 37°C for 10 min and fixed.

Croton oil–induced topical dermatitis. Croton oil experiments were performed as previously described(Schenkel et al., 2004). In brief, for pharmacologic studies, sex and age matched FVB/n mice were pretreated i.p. with anti-CD99 (clone 3F11; 5 mg antibody/kg animal), KH7 (5 μmol drug/kg animal), or DMSO (carrier control). 1 h later, 1% croton oil (Sigma-Aldrich) in a 9:1 mixture of acetone/olive oil (carrier) was applied to the left ears of animals. The right, contralateral ear was treated with carrier solution alone. After 5 h, the animals were sacrificed. For restoration experiments, after 3 h mice were injected i.p. with dimaprit (10 mg drug/kg animal; Bastaki et al., 2008) or H_2O (carrier). Control mice were sacrificed at this time to assess efficacy of anti-CD99 blockade at the time dimaprit was administered. Mice were then sacrificed 2 h later.

For transgenic studies, the ears of sex- and age-matched mice were stimulated as described above. Animals were sacrificed 5 h later. Before sacrifice, peripheral blood was collected. After sacrifice, cardiac tissue was harvested and MHEC were isolated as described above. FACS was performed on isolated leukocytes and MHEC to assess gene expression in each cell type.

The ears were harvested and fixed in 4% paraformaldehyde overnight at 4°C. Tissue was permeabilized and blocked in a solution of 0.3% Triton X-100, 2.5% BSA, and 2.5% host-species serum in PBS overnight at 4°C. Ears were then incubated in primary antibody (anti-PECAM (clone 2H8), anti-MRP14 (Abcam), anti-collagen IV (Abcam) in blocking solution overnight at 4°C. Tissue was incubated with secondary antibody (Dylight550 goat anti–Armenian hamster, Alexa Fluor 488 goat anti–rat, Alexa Fluor 647 goat anti–rabbit) in PBS for 4 h at RT. Tissue was mounted and postcapillary venules 20–40 mm were imaged using an Ultraview Vox imaging system equipped with a Yokogawa CSU-1 spinning disk and a 40× oil-immersion objective (na = 1.00). Images were analyzed using Volocity software (Perkin Elmer) which renders the optical sections into 3-dimensional images, allowing the localization of leukocytes relative to the ECs and basement membrane.

FACS. MHECs and mouse peripheral blood leukocytes were isolated from sAC-$C2^{flox/flox}$ and sAC-$C2^{flox/flox}$, VE-Cre^{+} mice as described above. For both cell types, RBCs were lysed for 15 min at room temperature, washed twice, and then incubated with rat anti–mouse CD16/CD32 (eBioscience) for 15 min at room temperature to block Fc receptors and washed twice more. Heart tissue homogenate was then labeled with FITC rat anti–mouse CD31 and APC rat anti–mouse CD45, or isotype control, for 30 min at 4°C. Mouse leukocytes were labeled with PE rat anti–mouse Ly6G (Gr1) and FITC rat anti–mouse CD31, or isotype control. Cells were then sorted at the Northwestern University Robert H. Lurie Comprehensive Cancer Center Flow Cytometry Core Facility using a FACSAria SORP 4-laser cell sorter (BD). MHEC were deemed those FITC $CD31^{+}$/APC $CD45^{-}$ in the heart tissue homogenate. Leukocytes were deemed those PE $Ly6G^{+}$/APC $CD45^{+}$ in the peripheral blood.

Genotyping of MHECs and mouse leukocytes. Genomic DNA was then extracted from MHEC and leukocyte populations using the DNeasy Blood & Tissue kit (QIAGEN). PCR genotyping of wild type and sAC-C2 KO alleles was performed using previous published primers (forward, 5′-GGACAGAAAGTAGAATGACTATCCCCCATTG-3′; reverse, 5′-CCGCTCACCTCTTTTCGGATTACATC-3′; Chen et al., 2013).

Statistical analysis. Numerical values represent the mean of at least three independent experiments ± SD (immunoblots) or SEM (TEM assays, TR assays, bead recruitment assays, and croton oil experiments). Variance of mean values between two groups were analyzed by the Student's *t* test for unpaired observations. Group differences were tested with one-way ANOVA (or two-way ANOVA when appropriate) followed by the Bonferroni's multiple comparison post-hoc test to calculate p-values. *, $P < 0.05$; **, $P < 0.01$; ***, $P < 0.001$; and ****, $P < 0.0001$. Statistical analyses were performed using GraphPad Prism software (GraphPad).

We would like to thank Dr. Clifford D. Carpenter for assistance with experiments and Drs. David P. Sullivan, Richard Miller, and Paul Bryce for insightful discussions. We would also like to thank Dr. Katia Scotlandi for providing the CD99 and scrambled shRNA constructs. We very much appreciate the help of the Northwestern University Genomics Core Facility for all their help in sequencing the constructs used. We would also like to thank the Northwestern University Robert H. Lurie Comprehensive Cancer Center Flow Cytometry Core Facility, specifically Paul Mehl, with their help in FACS analysis for our knockout mouse studies.

This work was supported by National Institutes of Health (NIH) NHLBI F30 HL116100-01A1 (to R.L. Watson) and NIH R37 HL064774 and R01 HL046849 (to W.A. Muller), and R01 GM62328 and R01 GM107442 (to L.R. Levin and J. Buck). Publication of this research was supported by the Sidney & Bess Eisenberg Memorial Fund.

Drs. Buck and Levin own equity interest in CEP Biotech, which has licensed commercialization of a panel of monoclonal antibodies directed against sAC. The authors declare no additional competing financial interests.

Submitted: 26 February 2015
Accepted: 14 May 2015

REFERENCES

Alcaide, P., S. Auerbach, and F.W. Luscinskas. 2009. Neutrophil recruitment under shear flow: it's all about endothelial cell rings and gaps. *Microcirculation*. 16:43–57. http://dx.doi.org/10.1080/10739680802273892

Ali, J., F. Liao, E. Martens, and W.A. Muller. 1997. Vascular endothelial cadherin (VE-cadherin): cloning and role in endothelial cell-cell adhesion. *Microcirculation*. 4:267–277. http://dx.doi.org/10.3109/10739689709146790

Alva, J.A., A.C. Zovein, A. Monvoisin, T. Murphy, A. Salazar, N.L. Harvey, P. Carmeliet, and M.L. Iruela-Arispe. 2006. VE-Cadherin-Cre-recombinase transgenic mouse: a tool for lineage analysis and gene deletion in endothelial cells. *Dev. Dyn.* 235:759–767. http://dx.doi.org/10.1002/dvdy.20643

Ancuta, P., R. Rao, A. Moses, A. Mehle, S.K. Shaw, F.W. Luscinskas, and D. Gabuzda. 2003. Fractalkine preferentially mediates arrest and migration of CD16+ monocytes. *J. Exp. Med.* 197:1701–1707. http://dx.doi.org/10.1084/jem.20022156

Banting, G.S., B. Pym, S.M. Darling, and P.N. Goodfellow. 1989. The *MIC2* gene product: epitope mapping and structural prediction analysis define an integral membrane protein. *Mol. Immunol.* 26:181–188. http://dx.doi.org/10.1016/0161-5890(89)90100-4

Bastaki, S.M., I.S. Chandranath, and J. Singh. 2008. The anti-secretory and anti-ulcer activities of esomeprazole in comparison with omeprazole in the stomach of rats and rabbits. *Mol. Cell. Biochem.* 309:167–175. http://dx.doi.org/10.1007/s11010-007-9657-5

Bitterman, J.L., L. Ramos-Espiritu, A. Diaz, L.R. Levin, and J. Buck. 2013. Pharmacological distinction between soluble and transmembrane adenylyl cyclases. *J. Pharmacol. Exp. Ther.* 347:589–598. http://dx.doi.org/10.1124/jpet.113.208496

Bixel, G., S. Kloep, S. Butz, B. Petri, B. Engelhardt, and D. Vestweber. 2004. Mouse CD99 participates in T-cell recruitment into inflamed skin. *Blood.* 104:3205–3213. http://dx.doi.org/10.1182/blood-2004-03-1184

Bixel, M.G., H. Li, B. Petri, A.G. Khandoga, A. Khandoga, A. Zarbock, K. Wolburg-Buchholz, H. Wolburg, L. Sorokin, D. Zeuschner, et al. 2010. CD99 and CD99L2 act at the same site as, but independently of, PECAM-1 during leukocyte diapedesis. *Blood.* 116:1172–1184. http://dx.doi.org/10.1182/blood-2009-12-256388

Buck, J., M.L. Sinclair, L. Schapal, M.J. Cann, and L.R. Levin. 1999. Cytosolic adenylyl cyclase defines a unique signaling molecule in mammals. *Proc. Natl. Acad. Sci. USA.* 96:79–84. http://dx.doi.org/10.1073/pnas.96.1.79

Butt, E., K. Abel, M. Krieger, D. Palm, V. Hoppe, J. Hoppe, and U. Walter. 1994. cAMP- and cGMP-dependent protein kinase phosphorylation sites of the focal adhesion vasodilator-stimulated phosphoprotein (VASP) in vitro and in intact human platelets. *J. Biol. Chem.* 269:14509–14517.

Carnegie, G.K., C.K. Means, and J.D. Scott. 2009. A-kinase anchoring proteins: from protein complexes to physiology and disease. *IUBMB Life.* 61:394–406. http://dx.doi.org/10.1002/iub.168

Cauthron, R.D., K.B. Carter, S. Liauw, and R.A. Steinberg. 1998. Physiological phosphorylation of protein kinase A at Thr-197 is by a protein kinase A kinase. *Mol. Cell. Biol.* 18:1416–1423.

Chen, J., J. Martinez, T.A. Milner, J. Buck, and L.R. Levin. 2013. Neuronal expression of soluble adenylyl cyclase in the mammalian brain. *Brain Res.* 1518:1–8. http://dx.doi.org/10.1016/j.brainres.2013.04.027

Dufour, E.M., A. Deroche, Y. Bae, and W.A. Muller. 2008. CD99 is essential for leukocyte diapedesis in vivo. *Cell Commun. Adhes.* 15:351–363. http://dx.doi.org/10.1080/15419060802442191

Ellis, N.A., T.Z. Ye, S. Patton, J. German, P.N. Goodfellow, and P. Weller. 1994. Cloning of *PBDX*, an *MIC2*-related gene that spans the pseudoautosomal boundary on chromosome Xp. *Nat. Genet.* 6:394–400. http://dx.doi.org/10.1038/ng0494-394

Farrell, J., L. Ramos, M. Tresguerres, M. Kamenetsky, L.R. Levin, and J. Buck. 2008. Somatic 'soluble' adenylyl cyclase isoforms are unaffected in Sacy tm1Lex/Sacy tm1Lex 'knockout' mice. *PLoS ONE.* 3:e3251. http://dx.doi.org/10.1371/journal.pone.0003251

Feng, D., J.A. Nagy, J. Hipp, H.F. Dvorak, and A.M. Dvorak. 1996. Vesiculovacuolar organelles and the regulation of venule permeability to macromolecules by vascular permeability factor, histamine, and serotonin. *J. Exp. Med.* 183:1981–1986. http://dx.doi.org/10.1084/jem.183.5.1981

Feng, G., D.P. Sullivan, F. Han, and W.A. Muller. 2015. Segregation of VE-cadherin from the LBRC depends on the ectodomain sequence required for homophilic adhesion. *J. Cell Sci.* 128:576–588. http://dx.doi.org/10.1242/jcs.159053

Ferraris, J.D., P. Persaud, C.K. Williams, Y. Chen, and M.B. Burg. 2002. cAMP-independent role of PKA in tonicity-induced transactivation of tonicity-responsive enhancer/osmotic response element-binding protein. *Proc. Natl. Acad. Sci. USA.* 99:16800–16805. http://dx.doi.org/10.1073/pnas.222659799

Forte, J.G., and L. Zhu. 2010. Apical recycling of the gastric parietal cell H,K-ATPase. *Annu. Rev. Physiol.* 72:273–296. http://dx.doi.org/10.1146/annurev-physiol-021909-135744

Fukuhra, S., A. Sakurai, A. Yamagishi, K. Sako, and N. Mochizuki. 2006. Vascular endothelial cadherin-mediated cell-cell adhesion regulated by a small GTPase, Rap1. *J. Biochem. Mol. Biol.* 39:132–139. http://dx.doi.org/10.5483/BMBRep.2006.39.2.132

Geng, W., Z. Wang, J. Zhang, B.Y. Reed, C.Y. Pak, and O.W. Moe. 2005. Cloning and characterization of the human soluble adenylyl cyclase. *Am. J. Physiol. Cell Physiol.* 288:C1305–C1316. http://dx.doi.org/10.1152/ajpcell.00584.2004

Gonzalez, G.A., and M.R. Montminy. 1989. Cyclic AMP stimulates somatostatin gene transcription by phosphorylation of CREB at serine 133. *Cell.* 59:675–680. http://dx.doi.org/10.1016/0092-8674(89)90013-5

Howe, A.K., L.C. Baldor, and B.P. Hogan. 2005. Spatial regulation of the cAMP-dependent protein kinase during chemotactic cell migration. *Proc. Natl. Acad. Sci. USA.* 102:14320–14325. http://dx.doi.org/10.1073/pnas.0507072102

Jaiswal, B.S., and M. Conti. 2001. Identification and functional analysis of splice variants of the germ cell soluble adenylyl cyclase. *J. Biol. Chem.* 276:31698–31708. http://dx.doi.org/10.1074/jbc.M011698200

Jarnaess, E., and K. Taskén. 2007. Spatiotemporal control of cAMP signalling processes by anchored signalling complexes. *Biochem. Soc. Trans.* 35:931–937. http://dx.doi.org/10.1042/BST0350931

Kim, C., N.H. Xuong, and S.S. Taylor. 2005a. Crystal structure of a complex between the catalytic and regulatory (RIalpha) subunits of PKA. *Science.* 307:690–696. http://dx.doi.org/10.1126/science.1104607

Kim, I., O.H. Yilmaz, and S.J. Morrison. 2005b. CD144 (VE-cadherin) is transiently expressed by fetal liver hematopoietic stem cells. *Blood.* 106:903–905.

Ley, K., C. Laudanna, M.I. Cybulsky, and S. Nourshargh. 2007. Getting to the site of inflammation: the leukocyte adhesion cascade updated. *Nat. Rev. Immunol.* 7:678–689. http://dx.doi.org/10.1038/nri2156

Liao, F., H.K. Huynh, A. Eiroa, T. Greene, E. Polizzi, and W.A. Muller. 1995. Migration of monocytes across endothelium and passage through extracellular matrix involve separate molecular domains of PECAM-1. *J. Exp. Med.* 182:1337–1343. http://dx.doi.org/10.1084/jem.182.5.1337

Lim, Y.C., G. Garcia-Cardena, J.R. Allport, M. Zervoglos, A.J. Connolly, M.A. Gimbrone Jr., and F.W. Luscinskas. 2003. Heterogeneity of endothelial cells from different organ sites in T-cell subset recruitment. *Am. J. Pathol.* 162:1591–1601. http://dx.doi.org/10.1016/S0002-9440(10)64293-9

Lou, O., P. Alcaide, F.W. Luscinskas, and W.A. Muller. 2007. CD99 is a key mediator of the transendothelial migration of neutrophils. *J. Immunol.* 178:1136–1143. http://dx.doi.org/10.4049/jimmunol.178.2.1136

Mamdouh, Z., X. Chen, L.M. Pierini, F.R. Maxfield, and W.A. Muller. 2003. Targeted recycling of PECAM from endothelial surface-connected compartments during diapedesis. *Nature.* 421:748–753. http://dx.doi.org/10.1038/nature01300

Mamdouh, Z., G.E. Kreitzer, and W.A. Muller. 2008. Leukocyte transmigration requires kinesin-mediated microtubule-dependent membrane trafficking from the lateral border recycling compartment. *J. Exp. Med.* 205:951–966. http://dx.doi.org/10.1084/jem.20072328

Mamdouh, Z., A. Mikhailov, and W.A. Muller. 2009. Transcellular migration of leukocytes is mediated by the endothelial lateral border recycling compartment. *J. Exp. Med.* 206:2795–2808. http://dx.doi.org/10.1084/jem.20082745

Manes, T.D., and J.S. Pober. 2011. Identification of endothelial cell junctional proteins and lymphocyte receptors involved in transendothelial migration of human effector memory CD4+ T cells. *J. Immunol.* 186:1763–1768. http://dx.doi.org/10.4049/jimmunol.1002835

Muller, W.A. 2011. Mechanisms of leukocyte transendothelial migration. *Annu. Rev. Pathol.* 6:323–344. http://dx.doi.org/10.1146/annurev-pathol-011110-130224

Muller, W.A., and F.W. Luscinskas. 2008. Assays of transendothelial migration in vitro. *Methods Enzymol.* 443:155–176. http://dx.doi.org/10.1016/S0076-6879(08)02009-0

Muller, W.A., and S.A. Weigl. 1992. Monocyte-selective transendothelial migration: dissection of the binding and transmigration phases by an in vitro assay. *J. Exp. Med.* 176:819–828. http://dx.doi.org/10.1084/jem.176.3.819

Muller, W.A., C.M. Ratti, S.L. McDonnell, and Z.A. Cohn. 1989. A human endothelial cell-restricted, externally disposed plasmalemmal protein enriched in intercellular junctions. *J. Exp. Med.* 170:399–414. http://dx.doi.org/10.1084/jem.170.2.399

Niu, J., R. Vaiskunaite, N. Suzuki, T. Kozasa, D.W. Carr, N. Dulin, and T.A. Voyno-Yasenetskaya. 2001. Interaction of heterotrimeric G13 protein with an A-kinase-anchoring protein 110 (AKAP110) mediates cAMP-independent PKA activation. *Curr. Biol.* 11:1686–1690.

Noda, K., J. Zhang, S. Fukuhara, S. Kunimoto, M. Yoshimura, and N. Mochizuki. 2010. Vascular endothelial-cadherin stabilizes at cell-cell junctions by anchoring to circumferential actin bundles through alpha- and beta-catenins in cyclic AMP-Epac-Rap1 signal-activated endothelial cells. *Mol. Biol. Cell.* 21:584–596. http://dx.doi.org/10.1091/mbc.E09-07-0580

Osawa, H., C.A. Smith, Y.S. Ra, P. Kongkham, and J.T. Rutka. 2009. The role of the membrane cytoskeleton cross-linker ezrin in medulloblastoma cells. *Neuro-oncol.* 11:381–393. http://dx.doi.org/10.1215/15228517-2008-110

Park, S.H., Y.K. Shin, Y.H. Suh, W.S. Park, Y.L. Ban, H.S. Choi, H.J. Park, and K.C. Jung. 2005. Rapid divergency of rodent CD99 orthologs: implications for the evolution of the pseudoautosomal region. *Gene*. 353:177–188. http://dx.doi.org/10.1016/j.gene.2005.04.023

Paunescu, T.G., N. Da Silva, L.M. Russo, M. McKee, H.A. Lu, S. Breton, and D. Brown. 2008. Association of soluble adenylyl cyclase with the V-ATPase in renal epithelial cells. *Am. J. Physiol. Renal Physiol.* 294:F130–F138. http://dx.doi.org/10.1152/ajprenal.00406.2007

Schenkel, A.R., Z. Mamdouh, X. Chen, R.M. Liebman, and W.A. Muller. 2002. CD99 plays a major role in the migration of monocytes through endothelial junctions. *Nat. Immunol.* 3:143–150. http://dx.doi.org/10.1038/ni749

Schenkel, A.R., T.W. Chew, and W.A. Muller. 2004. Platelet endothelial cell adhesion molecule deficiency or blockade significantly reduces leukocyte emigration in a majority of mouse strains. *J. Immunol.* 173:6403–6408. http://dx.doi.org/10.4049/jimmunol.173.10.6403

Schnoor, M., F.P. Lai, A. Zarbock, R. Kläver, C. Polaschegg, D. Schulte, H.A. Weich, J.M. Oelkers, K. Rottner, and D. Vestweber. 2011. Cortactin deficiency is associated with reduced neutrophil recruitment but increased vascular permeability in vivo. *J. Exp. Med.* 208:1721–1735. http://dx.doi.org/10.1084/jem.20101920

Seidman, M.A., T.W. Chew, A.R. Schenkel, and W.A. Muller. 2009. PECAM-independent thioglycollate peritonitis is associated with a locus on murine chromosome 2. *PLoS ONE*. 4:e4316. http://dx.doi.org/10.1371/journal.pone.0004316

Suh, Y.H., Y.K. Shin, M.C. Kook, K.I. Oh, W.S. Park, S.H. Kim, I.S. Lee, H.J. Park, T.L. Huh, and S.H. Park. 2003. Cloning, genomic organization, alternative transcripts and expression analysis of CD99L2, a novel paralog of human CD99, and identification of evolutionary conserved motifs. *Gene*. 307:63–76. http://dx.doi.org/10.1016/S0378-1119(03)00401-3

Sullivan, D.P., M.A. Seidman, and W.A. Muller. 2013. Poliovirus receptor (CD155) regulates a step in transendothelial migration between PECAM and CD99. *Am. J. Pathol.* 182:1031–1042. http://dx.doi.org/10.1016/j.ajpath.2012.11.037

Taylor, S.S., P. Zhang, J.M. Steichen, M.M. Keshwani, and A.P. Kornev. 2013. PKA: lessons learned after twenty years. *Biochim. Biophys. Acta.* 1834:1271–1278. http://dx.doi.org/10.1016/j.bbapap.2013.03.007

Tresguerres, M., L.R. Levin, and J. Buck. 2011. Intracellular cAMP signaling by soluble adenylyl cyclase. *Kidney Int.* 79:1277–1288. http://dx.doi.org/10.1038/ki.2011.95

van Buul, J.D., and P.L. Hordijk. 2009. Endothelial adapter proteins in leukocyte transmigration. *Thromb. Haemost.* 101:649–655.

Vliem, M.J., B. Ponsioen, F. Schwede, W.J. Pannekoek, J. Riedl, M.R. Kooistra, K. Jalink, H.G. Genieser, J.L. Bos, and H. Rehmann. 2008. 8-pCPT-2′-O-Me-cAMP-AM: an improved Epac-selective cAMP analogue. *ChemBioChem*. 9:2052–2054. http://dx.doi.org/10.1002/cbic.200800216

Wang, J., I. Shiratori, J. Uehori, M. Ikawa, and H. Arase. 2013. Neutrophil infiltration during inflammation is regulated by PILRα via modulation of integrin activation. *Nat. Immunol.* 14:34–40. http://dx.doi.org/10.1038/ni.2456

Wong, W., and J.D. Scott. 2004. AKAP signalling complexes: focal points in space and time. *Nat. Rev. Mol. Cell Biol.* 5:959–970. http://dx.doi.org/10.1038/nrm1527

Wright, S.D., P.E. Rao, W.C. Van Voorhis, L.S. Craigmyle, K. Lida, M.A. Talle, E.F. Westberg, G. Goldstein, and S.C. Silverstein. 1983. Identification of the C3bi receptor of human monocytes and macrophages by using monoclonal antibodies. *Proc. Nat. Acad. Sci.* 80:5699-5703.

Yang, L., R.M. Froio, T.E. Sciuto, A.M. Dvorak, R. Alon, and F.W. Luscinskas. 2005. ICAM-1 regulates neutrophil adhesion and transcellular migration of TNF-alpha-activated vascular endothelium under flow. *Blood*. 106:584–592. http://dx.doi.org/10.1182/blood-2004-12-4942

Zaccolo, M. 2009. cAMP signal transduction in the heart: understanding spatial control for the development of novel therapeutic strategies. *Br. J. Pharmacol.* 158:50–60. http://dx.doi.org/10.1111/j.1476-5381.2009.00185.x

Zhang, Y., K. Ma, P. Sadana, F. Chowdhury, S. Gaillard, F. Wang, D.P. McDonnell, T.G. Unterman, M.B. Elam, and E.A. Park. 2006. Estrogen-related receptors stimulate pyruvate dehydrogenase kinase isoform 4 gene expression. *J. Biol. Chem.* 281:39897–39906. http://dx.doi.org/10.1074/jbc.M608657200

Zippin, J.H., Y. Chen, P. Nahirney, M. Kamenetsky, M.S. Wuttke, D.A. Fischman, L.R. Levin, and J. Buck. 2003. Compartmentalization of bicarbonate-sensitive adenylyl cyclase in distinct signaling microdomains. *FASEB J.* 17:82–84.